ELEMENTAL ABUNDANCES IN QSOS:

Star Formation and Galactic Nuclear Evolution at High Redshifts

Fred Hamann

Department of Astronomy, University of Florida, 211 Bryant Space Sciences Center,
Gainesville, FL 32611-2055; hamann@astro.ufl.edu (current)

and

Center for Astrophysics and Space Sciences, University of California, San Diego, La Jolla,
CA 92093-0424

Gary Ferland

Department of Physics and Astronomy, University of Kentucky, Lexington, KY 40506-0055;
gary@pa.uky.edu

and

Canadian Institute for Theoretical Astrophysics, University of Toronto, Toronto, ON,
Canada, M5S 3H8

KEY WORDS: quasars, metallicity, emission lines, absorption lines, cosmology

Shortened Title: ELEMENTAL ABUNDANCES IN QSOS

ABSTRACT

Quasar (or QSO) elemental abundances provide unique probes of high-redshift star formation and galaxy evolution. There is growing evidence from both the emission and intrinsic absorption lines that QSO environments have roughly solar or higher metallicities out to redshifts >4. The range is not well known, but solar to a few times solar appears to be typical. There is also evidence for higher metallicities in more luminous objects, and for generally enhanced N/C and Fe/α abundances compared to solar ratios.

These results identify QSOs with vigorous, high-redshift star formation – consistent with the early evolution of massive galactic nuclei or dense proto-galactic clumps. However, the QSOs offer new constraints. For example, 1) most of the enrichment and star formation must occur before the QSOs "turn on" or become observable, on time scales of $\lesssim$1 Gyr at least at the highest redshifts. 2) The tentative result for enhanced Fe/α suggests that the first local star formation began at least ~1 Gyr prior to the QSO epoch. 3) The star formation must ultimately be extensive in order to reach high metallicities, i.e. a substantial fraction of the local gas must be converted into stars and stellar remnants. The exact fraction depends on the shape of the initial mass function (IMF). 4) The highest derived metallicities require IMFs that are weighted slightly more toward massive stars than the in solar neighborhood. 5) High metallicities also require deep gravitational potentials. By analogy with the well-known mass–metallicity relation among low-redshift galaxies, metal-rich QSOs should reside in galaxies (or proto-galaxies) that are minimally as massive (or as tightly bound) as our own Milky Way.

Contents

1. Introduction

Quasi-stellar objects (QSOs or quasars) are valuable probes of the high-redshift Universe (Schneider 1998). Their most distant representatives are now measurable out to redshifts of $z \sim 5$ (Schneider, Schmidt & Gunn 1991, Sloan Digital Sky Survey press release 1998). In Big Bang cosmologies, these redshifts correspond to times when the Universe itself was just ~1 Gyr old (see Fig. 1).

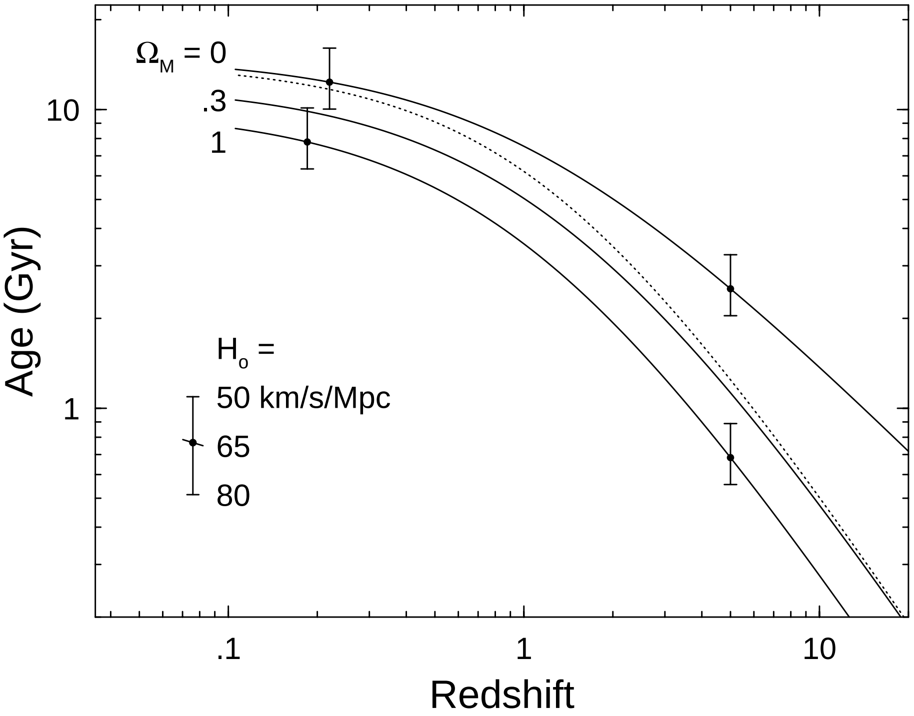

Fig. 1 — Redshift versus age of the Universe in Big Bang cosmologies. The three solid curves correspond to $H_o = 65$ km s^{-1} Mpc^{-1} and $\Omega_\Lambda = 0$ with $\Omega_M = 0$, 0.3 or 1. The dotted curve corresponds to $\Omega_\Lambda = 0.7$ and $\Omega_M = 0.3$. The "error" bars show the range of ages possible for H_o between 50 and 80 km s^{-1} Mpc^{-1} (see Carroll & Press 1992).

Understanding the elemental abundances in these distant, early-epoch environments is a major goal of quasar research. Some of the first spectroscopic studies noted simply that quasar environments contain the usual array of "metals" (elements C, N, O and heavier) produced by stellar nucleosynthesis (Shklovskii 1965, Burbidge & Burbidge 1967). More quantitative estimates of the abundances came later from theoretical work on the broad emission lines, culminating in the important review by Davidson & Netzer (1979 — hereafter DN79, also Baldwin & Netzer 1978, Shields 1976). Those studies inferred solar or slightly higher metal abundances, with large uncertainties. The past two decades have seen considerable progress. Today we have a better theoretical understanding of quasar environments, and greater abilities to both observe and model a range of abundance diagnostics.

We also have renewed motivation from the growing evidence that links quasars to galaxies. See, for example, Kormendy *et al.* (1998), Magorrian *et al.* (1998) for black hole–host galaxy mass correlations, Chatzichristou, Vanderriest & Jaffe (1999), Hines *et al.* (1999), McLeod, Rieke & Storrie-Lombardi (1999), Boyce, Disney & Bleaken (1999), McLure *et al.* (1998), Aretxaga, Terlevich & Boyle (1998), Carballo *et al.* (1998), Bahcall *et al.* (1997), Miller, Tran & Sheinis (1996), McLeod & Rieke (1995) for direct observations of QSO hosts, Cavaliere & Vittorini (1998), Shaver *et al.* (1998), Terlevich & Boyle (1993), Boyle & Terlevich (1998), Osmer (1998) for arguments based on QSO number-density evolution, McCarthy (1993), Saikia & Kulkarni (1998), Haas *et al.* (1998), Brotherton *et al.* (1998a) for radio galaxy–radio quasar unification schemes, and Turner (1991), Haehnelt & Rees (1993), Loeb & Rasio (1994), Katz *et al.* (1994), Haehnelt, Natarajan & Rees (1998), Haiman & Loeb (1998), Taniguchi, Ikeuchi & Shioya (1999) for theoretical links between QSOs and galaxy evolution. If quasars reside, as expected, in galactic nuclei or dense proto-galactic clumps, their abundances could yield unique constraints on the evolution of those environments. For example, quasar abundances can indirectly probe the star formation that came before QSOs, possibly the first stars forming in massive collapsed structures after the Big Bang. Other studies of high-redshift galaxies and metal enrichment, involving, for example, the "Lyman-break" objects (Steidel *et al.* 1998, Connolly *et al.* 1997) or the damped-Lyα or Lyα "forest" absorbers in QSO spectra (Pettini *et al.* 1997, Lu, Sargent & Barlow 1998, Rauch 1998), probe more extended structures. The quasar results should therefore provide an important piece to the overall puzzle of high-redshift star formation and galaxy evolution.

Here we review the status and implications of quasar abundance work. We regret that many interesting related topics must be excluded; in particular, we will consider the quasars themselves to be simply light sources surrounded by emitting and absorbing gas. We discuss three abundance diagnostics that are readily observable in QSOs at all redshifts: the broad emission lines (BELs), the broad absorption lines (BALs) and the intrinsic narrow absorption lines (NALs). We include just these "intrinsic" spectral features to probe the abundances near QSO engines — excluding measures of the extended host galaxies, nearby cluster galaxies or cosmologically intervening gas. We begin with separate discussions of each abundance probe (§§2–3), followed by a summary of the overall results (§4). We then consider the plausible enrichment schemes, making a case for normal chemical evolution by stars in galactic nuclei (§5). Within that scheme, we use results from galactic studies (§6) to derive further implications of the QSO abundances (§7). We close with a brief outline for future work (§8).

In several sections below we will present results of photoionization calculations performed with the numerical code Cloudy (version 90.05, Ferland *et al.* 1998). This code is freely available on the world wide web (http://www.pa.uky.edu/∼gary/cloudy/). Finally, we will define solar abundances according to the meteoritic results in Grevesse & Anders (1989).

2. Emission Line Diagnostics

2.1. Overview

Quasars are surprisingly alike in their emission-line spectra (Osmer & Shields 1999 and refs. therein); for example, the range of intensity ratios is far less than in galactic nebulae. Figure 2 shows a composite UV spectrum that is fairly typical of QSOs without strong BALs. The object-to-object similarities span the full range of QSO redshifts, $0.1 \lesssim z \lesssim 5$, more than 4 orders of magnitude in luminosity, and billions of years in cosmological look-back time. The emission lines are either insensitive to the metal abundances, or QSOs have similar abundances across enormous ranges in other parameters. We will argue that the truth involves a bit of both explanations.

We will focus on the BELs in the rest-frame UV because they are present and relatively easy to measure in all QSOs at all redshifts. Furthermore, unlike the narrow emission lines, there is no ambiguity about their close physical connection to QSO engines (DN79).

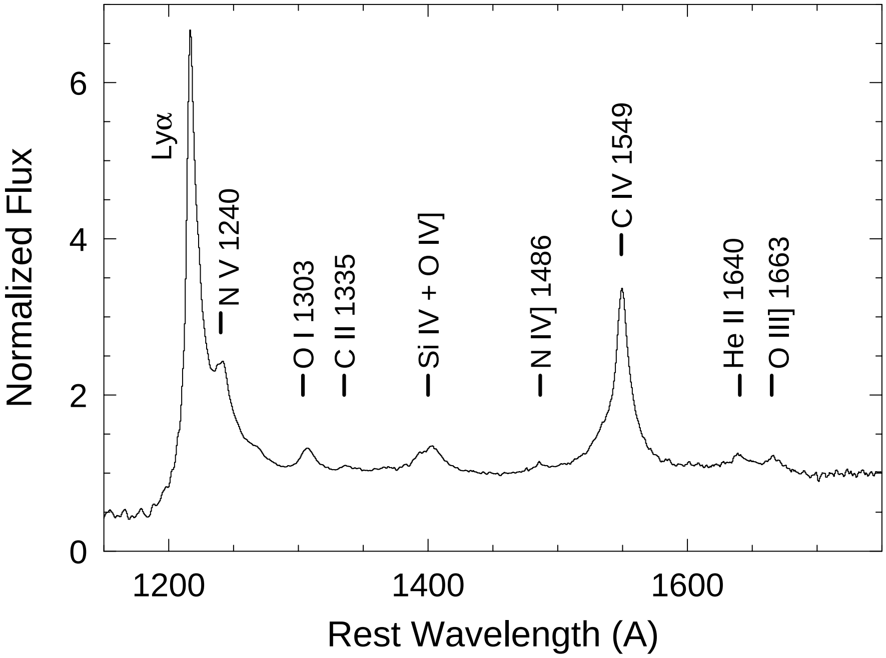

Fig. 2 — Normalized mean spectrum of 13 QSOs at $z > 4$ (from Shields *et al.* 1997). Prominent BELs are labeled.

2.2. Origin of the Broad Emission Lines

Quasar emission-line research is an example of the "inverse problem" in astrophysics. We know the answer — the observed spectrum of a quasar, and we are trying to understand the question — the conditions that created it. Any model of the line-forming regions will have uncertainties related to uniqueness, but these can be minimized by considering the astrophysical context and by limiting the models to essential properties. The essential properties of the BEL region (BELR) are as follows:

1) The BELR is photoionized. The main evidence for photoionization is that the emission-line spectra change in response to changes in the continuum, with lag-times corresponding to characteristic radii of the BELR (Peterson 1993). The shape of the ionizing continuum is a fundamental parameter and is in itself an area of active research (e.g. Zheng *et al.* 1997; Korista, Baldwin & Ferland 1997a, Brunner *et al.* 1997, Laor 1998). We will present calculations using simple power-laws between 1 μm and 100 keV, and describe results that do not depend strongly on the continuum shape.

2) The BELR spans a range of distances from the central object. The line variability or "reverberation" studies just mentioned find different lag-times for different ions. Highly ionized species tend to lie closer to the continuum source. Overall, the radial distances scale with luminosity, such that $R \approx 0.1(L/10^{46}\text{ergs s}^{-1})^{1/2}$ pc is a typical value (Peterson 1993).

3) The BELR has a wide range of densities and ionization states. The range in ionization follows simply from the lines detected, from OI λ1303 to at least NeVIII λ774 (Hamann *et al.* 1998). The range in density comes mainly from the estimated radii and photoionization theory (e.g. Ferland *et al.* 1992). Clouds[1] with densities from 10^8 to $>10^{12}$ cm^{-3} may be present. Any given object could have a broad mixture of BELR properties (Baldwin *et al.* 1995, 1996).

4) The BELR probably has large column densities. Large columns, typically $N_H \gtrsim 10^{23}$ cm^{-2}, were originally used in BELR simulations to produce a wide range of ionizations in single clouds (Kwan & Krolick 1981 — hereafter KK81, Ferland & Persson 1989). These large columns might not apply globally because we now know that different lines form in different regions. In our calculations below, we will truncate the clouds at the hydrogen recombination front, with the result that different clouds/calculations can have different total column densities. However, the truncation depths are in all cases large enough to include the full emission regions of the relevant lines.

5) Thermal velocities within clouds are believed to dominate the local line broadening and radiative transfer. The observed line-widths are thus due entirely to bulk motions of the gas. This issue is important because *i)* continuum photoexcitation ("pumping") can overwhelm other excitation processes if the local line broadening (e.g. micro-turbulence) is large, and *ii)* the line optical depths and thus photon escape probabilities (see below) vary inversely with the amount of line broadening. The interplay between these factors makes it hard to predict the behavior of a given line without explicit calculations. Shields, Ferland & Peterson (1995) plot some examples for the particular case of low column density clouds. One argument against significant micro-turbulence involves the Lyα/Hβ intensity ratio. Simple recombination theory predicts a ratio of about 34 (Osterbrock 1989 — hereafter O89) while the observed value is far smaller, closer to 10 (Baldwin 1977a). This discrepancy is worsened by micro-turbulence (Ferland 1999). The solution probably

---

[1] We use the term "cloud" loosely, referring to some localized part of the BELR but not favoring any particular model or geometry (see Arav *et al.* 1998, Mathews & Capriotti 1985).

requires severely trapped Lyα photons resulting from large optical depths at thermal line widths (see also Netzer *et al.* 1995).

2.3. Strategies for Abundance Work.

There is much that is unknown about QSO line-forming regions. We do not, for example, have a clear picture of the overall geometry or the spatial variations of key parameters; but we do not need this information for abundance work. The emission lines from photoionized clouds are controlled fundamentally by the energy balance and microphysics. The strategy for abundance studies is to identify line ratios that have significant abundance sensitivities and minimal dependences on other unknown or uncertain parameters. For example, we can minimize the sensitivity to large-scale geometric effects by comparing lines that form as much as possible in the same gas. Detailed simulations are often needed to identify useful line ratios and quantify their parameter sensitivities. Simple analytic expressions can be used for some applications and they can help, in any case, provide physical insight into the emission-line behaviors.

Below we review some of the basic principles of photoionization and emission-line formation. See O89 and Mihalas (1978) for further reviews, Davison & Netzer (1979 — hereafter DN79), KK81, Ferland & Shields 1985, and Netzer (1990 — hereafter N90) for applications to QSOs, and Ferland *et al.* (1998) for more on the numerical simulations and input atomic data.

2.4. Basics of Abundance Analysis

2.4.1. Collisionally-Excited Lines

Collisionally-excited lines form by the internal excitation of an ion following electron impact. Their emissivities, or energy released per unit volume and time, follow from the statistical equilibrium of the energy levels. For example, the equilibrium (detailed balance) equation for a 2-level atom is,

$$n_l n_e q_{lu} \;=\; n_u(\beta A_{ul} + n_e q_{ul}) \qquad [\mathrm{cm^{-3}\ s^{-1}}] \tag{1}$$

where n_e is the electron density, β is the probability for line photons escaping the local region ($0 \leq \beta \leq 1$), A_{ul} is the spontaneous decay rate, n_u and n_l are the number densities in the upper and lower states, and q_{lu} and q_{ul} are the upward and downward collisional rate coefficients, respectively. Note that $\beta \sim \tau^{-1}$ when $\tau \gg 1$, where τ is the line-center optical depth (Frisch 1984). For most applications the ions are mainly in their ground state and n_l is approximately the ionic density. The line emissivity is,

$$\epsilon_{coll} \;=\; n_u \beta A_{ul} h\nu_o \;=\; n_l \beta A_{ul} h\nu_o \left(\frac{n_e q_{lu}}{\beta A_{ul} + n_e q_{ul}}\right) \qquad [\mathrm{ergs\ cm^{-3}\ s^{-1}}] \tag{2}$$

where ν_o is the line frequency. This emissivity has a strong temperature dependence because $q_{ul} \propto T^{-1/2}$ and $(q_{lu}/q_{ul}) = (g_u/g_l)\exp(-h\nu_o/kT)$, where g_u and g_l are the statistical weights. In the high density limit we have,

$$\epsilon_{coll} \;=\; n_l \beta A_{ul} h\nu_o \, \frac{g_l}{g_u} \, \exp\left(-\frac{h\nu_o}{kT}\right) \qquad (3)$$

and the levels are said to be "thermalized." Line thermalization, where ϵ_{coll} no longer depends on the transition strength, additionally requires $\tau \gg 1$. (A_{ul} and τ are both proportional to the oscillator strength, which therefore drops out of the factor $\beta A_{ul} \approx A_{ul}/\tau$ in Eqn. 3 if $\tau \gg 1$.) At low densities we have,

$$\epsilon_{coll} \;=\; n_l n_e q_{lu} h\nu_o \;\propto\; n_l n_e T^{-1/2} \, \exp\left(-\frac{h\nu_o}{kT}\right) \qquad (4)$$

Note that ϵ_{coll} scales here like the density squared, compared to the linear dependence in Equation 3. The critical density, n_{crit}, between these two limits is the density where the two terms in the denominator of Equation 2 are equal,

$$n_{crit} \;=\; \frac{\beta A_{ul}}{q_{ul}} \approx \frac{A_{ul}}{\tau q_{ul}} \qquad (5)$$

where the approximate relation holds only if $\tau \gg 1$. Physically n_{crit} is the density where the upper level is as likely to be de-excited by collisions as by radiative decays. Note that significant optical depths have the effect of lowering n_{crit}. Also note that transitions with very different oscillator strengths (but similar collision strengths) will have similar n_{crit} in the limit $\tau \gg 1$ (because A_{ul}/τ is independent of oscillator strength).

2.4.2. Recombination Lines

The most prominent recombination lines belong to HI, HeI and HeII, with HI Lyα being typically strongest. These lines form by the capture of free electrons into excited states, followed by radiative decays to lower states. In the simplest case, where every photon escapes freely and competing processes are unimportant, the emissivity is,

$$\epsilon_{rec} \;=\; n_i \, n_e \, \alpha_{rad} \, h\nu_o \;\propto\; n_i \, n_e T^{-1} \qquad [\mathrm{ergs\ cm^{-3}\ s^{-1}}] \qquad (6)$$

where α_{rad} is the radiative recombination coefficient into the upper energy state and n_i is the number density of parent ions. The temperature dependence is approximate and derives from α_{rad} (see O89).

2.4.3. Deriving Abundance Ratios

These two types of lines can be combined to form three types of ratios for abundance analysis. The general idea is that for any element a in ion stage i, the observed line intensity, $I(a_i)$, is proportional to the density in that ion, $n(a_i)$, times a function of the overall gas density and temperature, $F(a_i, T, n)$, such that $I(a_i) = n(a_i)F(a_i, T, n)$. The ionic abundance ratios are then given by,

$$\frac{n(a_i)}{n(b_j)} \;=\; \frac{I(a_i)}{I(b_j)} \, \frac{F(b_j, T, n)}{F(a_i, T, n)} \qquad (7)$$

Abundance studies require line pairs for which the ratio of the two functions F is nearly constant or has limiting behaviors that still allow for abundance constraints. The last step is to convert the ionic abundances into elemental abundances, which we express logarithmically relative to solar ratios as[2],

$$\left[\frac{a}{b}\right] \;=\; \log\left(\frac{n(a_i)}{n(b_j)}\right) \;+\; \log\left(\frac{f(b_j)}{f(a_i)}\right) \;+\; \log\left(\frac{b}{a}\right)_{\odot} \tag{8}$$

where $f(a_i)$ is the fraction of element a in ion stage i, etc. The middle term on the right hand side is the ionization correction (IC), which can be deduced from numerical simulations or set to zero (in the log) based on the similarity of the species (Peimbert 1967). Another strategy is to compare summed combinations of lines from different ion stages so that IC tends to zero on average (Davidson 1977).

Ratios of pure recombination lines are simplest because they are least sensitive to the temperature and density. In principle, we could derive the He/H abundance from these ratios. However, in practice, all of the strong HI and HeI recombination lines in QSOs, most notably Lyα, are affected by collisions and thermalization effects. Moreover, because H^o, He^+ and He^{+2} have different ionization energies, they need not be co-spatial in the BELR and their levels of ionization depend on the different numbers of photons available to produce each ion (Williams 1971). As a result, the H and He recombination spectra are most useful as indicators of the shape of the ionizing continuum (e.g. Korista *et al.* 1997a). We do not expect substantial deviations from solar He/H abundances anyway, based on normal galactic chemical evolution, and the BEL data are grossly consistent with that expectation.

The second possible ratio involves collisional to recombination lines. These ratios have strong temperature dependences (compare Eqns. 3 and 4 to Eqn. 6). Nonetheless, they can still be used for abundance work if the temperature sensitivities are quantified by explicit calculations. For example, there is an upper limit on the line ratio NV λ1240/HeII λ1640 related to the maximum temperature attained in photoionized BELRs. That upper limit sets a firm lower limit on the N/He abundance (§2.6.3 below).

The last ratio, and the one most often used, involves two collisionally-excited lines. Roughly a dozen collisionally-excited BELs are routinely measured in the UV spectra of quasars, so there are a variety of possibilities. The ideal collisionally-excited line pair would have similar excitation energies, so their ratio has a small $h\Delta\nu_o/kT$ and thus a small temperature dependence (Eqns. 3 and 4). Similar values of n_{crit} and similar ionization energies further minimize the sensitivities to density and BELR structure. Well-chosen ratios that meet these criteria can sometimes provide abundance estimates without recourse to detailed simulations (e.g. Shields 1976, §2.6.1 below)

---

[2] Our notation here is based on the usual definition of logarithmic abundances normalized to solar ratios, $[a/b] \equiv \log(a/b) - \log(a/b)_{\odot}$.

2.5. Photoionization Simulations

A photoionized cloud is essentially a large-scale fluorescence problem. Energy comes into the cloud via continuum radiation, is converted into kinetic energy by the photo-ejection of electrons, and then leaves the cloud by various emission processes – mainly line radiation. The lines are thus the primary coolants; their total intensity depends on energy conservation and not at all on particular cloud properties.

In general situations, e.g. dense environments like BELRs, individual line strengths can be governed by a number of competing processes and by feedback related to the cloud structure and energy balance. Detailed calculations are needed to simultaneously consider a complex network of coupled processes. Here we describe some basic results for the line formation and ionization structure in realistic BELR clouds.

2.5.1. Parameters of Photoionization Equilibrium

The fundamental parameters in photoionization simulations are the shape and intensity of the ionizing continuum, and the gas' space density, column density, and chemical composition. The flux of hydrogen-ionizing photons at the illuminated face of a cloud is,

$$\Phi(H) \equiv \int_{\nu_{LL}}^{\infty} \frac{f_\nu}{h\nu}\, d\nu \quad [\text{photons cm}^{-2}\ \text{s}^{-1}] \tag{9}$$

where f_ν is the energy flux density and ν_{LL} is the frequency corresponding to 1 Ryd. A dimensionless ionization parameter $U \equiv \Phi(H)/cn_H$ is often used instead, where c is the speed of light and n_H is the total hydrogen density (H^o + H^+). U is proportional to the level of ionization and has the advantage of stressing homology relations between clouds with the same U but different $\Phi(H)$ and n_H. This simplification is appropriate if we are interested in just the gross ionization structure or in emission lines that are not collisionally suppressed. More generally, we can use either $\Phi(H)$ or U as long as the density is also specified.

2.5.2. A Computed Structure

Figure 3 shows the ionization structure of a typical BELR cloud photoionized by a power-law spectrum with $\alpha = -1.5$, where $f_\nu \propto \nu^\alpha$. The hydrogen recombination front occurs at a depth of $\sim 10^{12}$ cm, while the He^{+2}–He^{+} front is near 10^{11} cm. Note that there is significant ionization beyond the nominal H^o–H^+ front, due to penetrating X-rays and Balmer continuum photoionizations out of the $n = 2$ level in H^o (KK81). Some important low-ionization lines like FeII form in that region. The ionization fractions in plots like Figure 3 help us identify ions, such as O^{+5}, N^{+4} and He^{+2}, that are roughly co-spatial and thus good candidates for abundance comparisons.

XXXXXX INSERT FIGURE HERE XXXXXX

Fig. 3 — Ionization structure for a nominal BELR cloud with $n_H = 10^{10}$ cm^{-3}, $\log U = -1.5$ and solar abundances.

2.5.3. An Example: the CIV λ1549 Equivalent Width

CIV λ1549 is one of the strongest collisionally-excited lines in quasar spectra. The left panel of Figure 4 shows how its predicted equivalent width changes with the density (n_H) and ionizing flux ($\Phi(H)$, see Korista *et al.* 1997b for many more similar plots). Powerful selection effects are clearly at work; the line radiates efficiently over just a narrow range of parameters. Varying $\Phi(H)$ is equivalent to moving the cloud closer or farther from the continuum source. The line is weak at large values of $\Phi(H)$, because carbon is too highly ionized, and at low values of $\Phi(H)$, because carbon is too neutral. The line strength also changes with the gas density. When the density is above n_{crit}, the line is collisionally suppressed and other permitted lines take over the cooling. When the density is low, the line weakens as the many forbidden and semi-forbidden lines become efficient coolants and the gas temperature declines. The line is most prominent at $n_H \approx 10^{10}$ cm^{-3} and $\log U \approx -1.5$, which are the canonical BELR parameters deduced over twenty years ago from analysis of the CIV emission (DN79).

XXXXXX INSERT FIGURE HERE XXXXXX

Fig. 4 — Predicted equivalent width (EW) of CIV λ1549 as a function of the cloud density, n_H, and incident ionizing flux, $\Phi(H)$. The equivalent width here is dimensionless (line flux/$\nu_o f_{\nu_o}$ in the continuum) and applies for the hypothetical case of global covering factor unity. Flux ratios for NV λ1240/HeII λ1640 and NV/CIV are also shown. Other parameters are the same as Fig. 3.

It is important to remember that these selection effects exist whenever we observe an emission line. Baldwin *et al.* (1995) showed that a typical quasar BEL spectrum might result simply from selection effects operating in BELRs with a wide range of cloud properties (e.g. density and distance from the QSO). Numerical simulations can identify pairs of lines with similar selection behaviors so that their ratios are insensitive to the ranges or specific values of the parameters.

2.5.4. Line Dependence on Continuum Shape

Figure 5 shows a series of calculations using different incident spectral shapes. The actual shape of the ionizing continua in QSOs is a complicated issue, but the UV to X-ray slopes are roughly consistent with $\alpha \sim -1.5$, near the center of the range shown (see Laor 1998, Korista *et al.* 1997a for recent discussions). The results in Figure 5 mainly reflect the conservation of energy in the cloud. Harder spectra (less negative α) provide more heating per photoionization, leading to higher temperatures. The increased heating requires more line cooling via collisionally-excited lines like CIV. The ratio of a collisionally-excited line to a recombination line, such as CIV/Lyα, is proportional to the cooling per recombination or equivalently the heating per photoionization (DN79). Such ratios therefore have a strong continuum-shape dependence. The strengths of collisionally-excited lines relative to the adjacent continuum (i.e. their equivalent widths) also depend on the spectral slope because of the temperature sensitivity and because the continuum below the lines might be very different from that controlling the ionization. Ratios of collisionally-excited lines, such as NV/CIV, can similarly depend on the spectral shape if their ionization or excitation energies are different. In dense BELRs, these simple behaviors can be moderated by other effects. For example, the Lyα equivalent width increases with spectral hardening at fixed U (Fig. 5) because it has a significant collisional (temperature-sensitive) contribution.

XXXXXX INSERT FIGURE HERE XXXXXX

Fig. 5 — Predicted line flux ratios, gas temperatures ($T_4 = T/10^4$ K in the O^{+2} zone, i.e. weighted by the O^{+2} fraction), and dimensionless equivalent widths in Lyα (EW, as in Fig. 4) are plotted for clouds photoionized by different power law spectra. Other parameters are the same as Fig. 3. The lines are CIII λ977, NIII λ991, OVI λ1034, NV λ1240, CIV λ1549, HeII λ1640, OIII] λ1664, NIII] λ1750 and CIII] λ1909.

2.5.5. Line Dependence on Abundances

The left-hand panel of Figure 6 shows a series of calculations for clouds with different metallicities, Z (scaled from solar and preserving solar ratios). The strengths of the collisionally-excited lines relative to Lyα change little with Z. In particular, CIV/Lyα varies negligibly for $0.1 \lesssim Z \lesssim 30$ $Z_\odot$ (see also Hamann & Ferland 1993a, hereafter HF93a). We have already noted that these ratios are more sensitive to the continuum shape (§2.5.4). Their lack of sensitivity to Z can be traced to feedback in the energy balance. As the metal abundances grow, the line cooling increases. The growing metallicities, which might otherwise increase the metal line strengths, are thus balanced in real clouds by lower temperatures — with the result that the total metal line flux stays constant. This feedback is especially important for strong lines, like CIV, that by themselves control a large fraction of the cooling. Weak lines respond better to abundance changes. At low metallicities ($Z \lesssim 0.02$ $Z_\odot$) none of the metal lines are important coolants and their overall strengths do scale with Z.

Another factor in the line behaviors at high Z is the increasing bound-free continuum absorption by metal ions. The metals absorb a larger fraction of the far-UV flux at high Z, such that the H and He recombination lines become somewhat weaker. This effect dominates the high-Z rise in OVI/HeII and NV/HeII in Figure 6.

The right-hand panel in Figure 6 shows the same line ratios as before, but in this case nitrogen is scaled such that N/H $\propto Z^2$ (where N/H is solar at $Z = Z_\odot$). This selective scaling is based on the expected secondary nucleosynthesis of nitrogen (§6 below). Shields (1976) noted that this abundance pattern should occur in QSOs by analogy with its direct observation in galactic HII regions. Figure 6 shows that it leads to a strong metallicity dependence for line ratios involving nitrogen. This strong dependence is possible because the N lines do not control the cooling.

XXXXXX INSERT FIGURE HERE XXXXXX

Fig. 6 — Predicted line flux ratios for photoionized clouds with different metallicities, Z. The metals are scaled together (preserving solar ratios) in the left-hand panel, while nitrogen is selectively scaled like Z^2 in the right panel. Other parameters are the same as Fig. 3. See Fig. 5 for line notations.

2.6. Abundance Diagnostics and Results

2.6.1. Intercombination Lines

Shields (1976) proposed using various collisionally-excited intercombination (semi-forbidden) lines to derive metal-to-metal abundance ratios in QSOs. He emphasized the strengths of NIII] λ1750 and NIV] λ1486 compared to OIII] λ1664, CIII] λ1909 and CIV λ1549 as potential diagnostics of the overall metallicity. As noted above, the metallicity dependence stems from the expected Z^2 scaling of N via secondary nucleosynthesis (also §6 below). Shields selected lines with similar ionization and excitation energies, so that their ratios are insensitive to the uncertain temperature, ionization and geometry. Comparisons with the measured line ratios in QSOs (see also Davidson 1977, Baldwin & Netzer 1978, DN79, Osmer 1980, Uomoto 1984) suggested that N/C and N/O are often solar or higher, consistent with solar or higher metallicities. Gaskell, Shields & Wampler (1981) extended this analysis to SiIII] λ1892 and other lines to show that the refractory elements cannot be substantially depleted by dust in BELRs.

One drawback of the intercombination lines is that most of them are weak and therefore difficult (or impossible) to measure. Nonetheless, the best recent measurements (Wills *et al.* 1995, Laor *et al.* 1995, Boyle 1990, Baldwin *et al.* 1996) support the earlier results. It is now possible to gather even more data for these lines at a range of redshifts. A note of caution is that the strong feature generally attributed to CIII] λ1909 can have large contributions from other lines (Laor *et al.* 1995, 1997, Baldwin *et al.* 1996), so that ratios like NIII]/CIII] might systematically underestimate N/C if line blending is not accounted for.

A more serious concern is that the early theoretical work did not consider the range of high densities now believed to be present in the BELR (§2.2). The intercombination lines probably form at or near their critical densities (typically 3×10^9 to 10^{11} cm^{-3} for $\beta = 1$ in Eqn. 5). Lines with different n_{crit} could have different degrees of collisional suppression. (For example, the calculated results using $n_e \approx n_H = 10^{10}$ cm^{-3} in Figs. 5 and 6 favor large NIII]/CIII] at a given N/C abundance because CIII] is collisionally suppressed above its $n_{crit} \approx 3 \times 10^9$ cm^{-3}.) If there is a range of densities, lines with different n_{crit} might form in different regions (even if they have similar ionizations), leading to a geometry dependence. Nonetheless, line ratios involving similar n_{crit} and similar sensitivities to other parameters, such as NIII]/OIII], could still be robust abundance indicators when they are measurable. More theoretical work is needed to explore the parameter sensitivities and selection effects that can influence these lines in complex BELRs.

2.6.2. Permitted Lines

There are several possibilities for abundance diagnostics among the permitted UV lines. Figure 6 shows that NIII λ991/CIII λ977 and NV λ1240/CIV λ1549 should be good tracers of N/C. Another possibility is NV/HeII λ1640, or perhaps NV/(CIV+OVI λ1034). The NV, OVI and HeII lines form in overlapping regions (Fig. 3), as do NIII and CIII, so their flux ratios should be insensitive to the global BELR structure. Also, as noted above, the N lines are not important coolants and thus responsive to abundance changes. There are practical problems with most of these lines, however; NV is blended with Lyα, CIII, NIII and HeII are weak, and CIII, NIII and OVI lie in the "forest" of intervening Lyα absorption lines. Nonetheless, improvements in the quality of data (for example, high resolution and high signal-to-noise spectra in the Lyα forest) are permitting increasingly accurate measurements of these lines in large QSO samples.

2.6.3. NV/HeII and NV/CIV

Some of the first studies of large QSO samples noted that NV λ1240 is often stronger than predicted by photoionization models using solar abundances (Osmer & Smith 1976 and 1977). The NV/HeII and NV/CIV ratios have since received particular attention as abundance diagnostics (Hamann & Ferland 1992, HF93a, Hamann & Ferland 1993b — hereafter HF93b, and Ferland *et al.* 1996 — hereafter F96). Figure 7 shows the measured ratios in these lines for QSOs at different redshifts (from HF93b and Hamann *et al.* 1997a, with some new data and modifications based mainly on Wills *et al.* 1995 and Baldwin *et al.* 1996). NV/HeII is the ratio of a collisional to recombination line, with the expected strong temperature dependence (§2.4). Calculations similar to (but more exhaustive than) those shown in Figures 4–6, indicate that NV/HeII reaches a maximum value linked to the maximum temperature in photoionized clouds (F96). The maximum NV/HeII ratio is ~2–3 for solar N/He abundances, depending on how "hard" a continuum shape one considers realistic for QSOs. (Beware that the highest ratios in Fig. 4 occur for parameters where both lines are growing weak, cf. the EW(CIV) plot or Korista *et al.* 1997b.) Nominal BELR parameters predict NV/HeII near unity for solar N/He (Figs. 4–6). These predictions fall well below most of the measured ratios (Fig. 7), implying that QSOs typically have super-solar N/He. The ad hoc (high) temperatures that would be needed to explain the observed NV/HeII ratios with solar N/He are inconsistent with photoionization equilibrium, and would lead to strong far-UV emission lines. The fact that these far-UV line strengths are not seen sets an upper limit on the temperature and supports the result for super-solar N/He (F96).

The NV/CIV lines are collisionally excited with similar energies, so the temperature dependence is smaller than NV/HeII. Nominal BELR parameters predict NV/CIV of order 0.1 for solar N/C (Figs. 4–6, also HF93a,b). Comparisons with the data in Figure 7 thus indicate super-solar N/C for most QSOs.

The two NV ratios together therefore imply that 1) quasar metallicities are often solar or higher, especially in high redshift, high luminosity objects, and 2) nitrogen (e.g. N/C) is typically enhanced compared to solar ratios (F96, HF93a,b). The conclusion for enhanced N/C is based largely on NV/CIV, but we note that the scaling of $N \propto Z^2$ leads to self-consistent estimates of Z based on NV/HeII and NV/CIV (Fig. 7). The actual Z values are uncertain, but the main point is that many observed ratios require $Z \gtrsim Z_\odot$. Figures 6 and 7 combined suggest that the nominal metallicity range is $1 \lesssim Z \lesssim 10\ Z_\odot$ for standard photoionization parameters and $N \propto Z^2$.

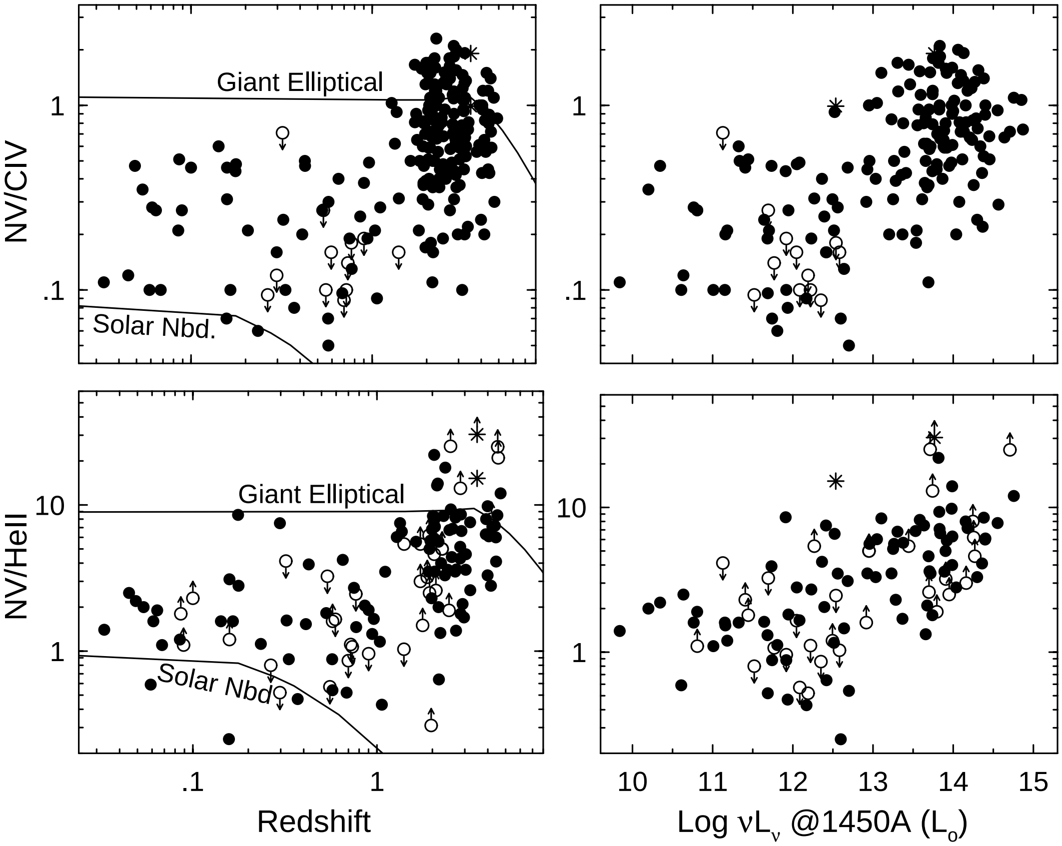

Fig. 7 — Measured NV/HeII and NV/CIV flux ratios versus redshift (left panels) and continuum luminosity (right). The upper and lower ranges might be undersampled (especially for NV/HeII at redshifts >1) because limits on weak lines (e.g. HeII) were often not available from the literature. The two asterisks in each panel represent mean values measured by Osmer *et al.* (1994) for "high" and "low" luminosity QSOs at redshift >3. The solid curves are predictions based on chemical evolution models (discussed in §6 below).

HF93b noted that the observed NV ratios tend to be higher in more luminous sources (Fig. 7). Most BELs exhibit the well-known "Baldwin effect," that is, lower equivalent widths at higher luminosities (Baldwin 1977b). This effect is well established in CIV and appears to be even stronger in OVI (Zheng *et al.* 1995, Kinney, Rivolo & Koratkar 1990, Osmer & Shields 1999). Surprisingly, NV does not show this effect (Osmer *et al.* 1994, Laor *et al.* 1995, Francis & Koratkar 1995) even though its ionization is intermediate between CIV and OVI and its electron structure is identical. We proposed that the peculiar NV behavior is due to generally higher metallicities and more enhanced N abundances in more luminous QSOs. The recent theoretical study of the Baldwin effect by Korista, Baldwin & Ferland (1998) gives quantitative support to that conclusion. In §7 we will argue that this proposed metallicity–luminosity trend in QSOs could naturally result from a mass–metallicity correlation among their host galaxies.

The abundance results based on NV have been questioned by Turnshek *et al.* (1988, 1996) and Krolik & Voit (1998), who argue that the NV BEL forms largely by resonance scattering in an outflowing BAL region. NV might be selectively enhanced by this mechanism because it can scatter both the continuum and the underlying Lyα emission line. However, explicit calculations of the line scattering (Hamann, Korista & Morris 1993, Hamann & Korista 1996, Hamann, Korista & Ferland 1999a) do not support this scenario. For example, 1) the amount of NV scattering estimated by Krolik & Voit (1998) is too large by a factor of $\sim$3 on average, because BALRs do not generally have the right velocity/optical depth structure to scatter all of the incident Lyα photons. In particular, NV BALs are not usually black across the Lyα emission line. 2) It is difficult for NV ions in high-velocity BAL winds to scatter Lyα photons into simple emission profiles with observed half-widths of typically 2000 to 2500 km s^{-1}. For example, isotropic scattering of the Lyα flux would produce BEL half-widths of $\sim$6000 km s^{-1} (the velocity separation between the NV and Lyα lines). Anisotropic scattering (e.g. in BALRs with equatorial or bipolar geometries) would lead to strong orientation effects and systematically broader BEL profiles in BAL versus non-BAL QSOs. These differences are not observed (Weymann *et al.* 1991). 3) It is not clear why, in individual spectra, the NV emission profiles should closely resemble those of other BELs if the former is produced by scattering in a high-velocity BAL wind while the latter are collisionally excited in a separate region (i.e. the usual BELR — whose velocity field is not mostly radial based on the reverberation studies, Türler & Courvoisier 1997, Korista *et al.* 1995). Finally, 4) large scattering contributions to NV would minimally require much larger global BALR covering factors (the fraction of the sky covered by the BALR as seen from the central QSO) than expected from their observed detection frequency in (randomly oriented) QSO samples. Goodrich (1997) and Krolik & Voit (1998) argue that larger global covering factors could occur, but that issue is not settled.

Another concern is that complex BELR geometries might cause the NV/HeII and NV/CIV abundance indicators to fail — but they would fail in opposite directions. Specifically, clouds that are truncated at different physical depths (see Fig. 3) could produce strong HeII with little or no NV and CIV emission, or strong HeII and NV with little or no CIV. For a given abundance set, this type of truncation could therefore either lower the observed NV/HeII ratio or increase NV/CIV. Comparing the data to simulations that do not take truncation into account (Figs. 4–6) might then lead to underestimated N/He abundances or overestimated N/C. However, we have already shown that these two line ratios yield similar metallicities when compared to the non-truncated simulations, so we are not likely being mislead by complex BELR geometries. Moreover, the NV/HeII ratio provides in any case a secure lower limit on N/He.

2.6.4. FeII/MgII

The broad FeII emission lines pose unique problems because the atomic physics is complex and many blended lines contribute to the spectrum, particularly at the wavelengths ∼2000–3000 Å and ∼4500–5500 Å. Nonetheless, FeII is worth the effort because a delay of ∼1 Gyr in the Fe enrichment, relative to α elements such as O, Mg or Si, might provide a "clock" for constraining the ages of QSOs and the epoch of their first star formation (see §§6–7 below, also HF93b).

A series of important papers on FeII emission (Osterbrock 1977, Phillips 1977,1978, Grandi 1981) culminated with Wills & Netzer (1983) and Wills, Netzer & Wills (1985, hereafter WNW). They performed sophisticated calculations showing that the large observed FeII fluxes, e.g. FeII(UV)/MgII λ2799, require that either Fe is several times overabundant (compared to solar ratios) or some unknown process dominates the FeII excitation. One process that might selectively enhance FeII emission is photoexcitation by Lyα photons (Johansson & Jordan 1984). The absorption of Lyα radiation can pump electrons from the lower (metastable) energy levels of Fe^{+} into specific high-energy states, leading to fluorescent cascades. WNW discounted this mechanism because it appeared insignificant in their simulations, but Penston (1987) noted that Lyα pumping is known to be important in some emission-line stars, such as the symbiotic star RR Tel, and therefore might be important in QSOs. More recent FeII simulations using better atomic data and exploring a wider range of physical conditions (Sigut & Pradhan 1998, Verner *et al.* 1999) suggest that Lyα can be important in some circumstances, but it is not yet clear if those circumstances occur significantly in QSOs.

Recent observations have renewed interest in this question by showing that the FeII(UV)/MgII emission fluxes can be larger than the WNW predictions even at $z > 4$, with the tentative conclusion that Fe/Mg is at least solar (and thus the objects are at least ∼1 Gyr old, Taniguchi *et al.* 1997, Yoshii, Tsujimoto & Kawara 1998, Thompson, Hill & Elston 1999 and refs. therein). New theoretical efforts, such as Sigut & Pradhan (1998) and Verner *et al.* (1999), are needed to test these conclusions and quantify the uncertainties. However, a better way to measure Fe/α might be with the intrinsic NALs (see below).

3. Absorption Line Diagnostics

3.1. Overview: Types of Absorption Lines

Quasar absorption lines can have a variety of intrinsic or cosmologically intervening origins. We exclude from our discussion the damped-Lyα absorbers and the "forest" of many narrow Lyα systems with weak or absent metal lines because they form in cosmologically intervening gas (Rauch 1998). The remaining metal-line systems can be divided into two classes according to their broad or narrow profiles. This division is a gross simplification, but still useful because it distinguishes the clearly intrinsic broad lines from the many others of uncertain origin. Here we briefly characterize the two (broad and narrow) line types.

3.1.1. Broad Absorption Lines (BALs)

Broad absorption lines are blueshifted with respect to the emission lines and have velocity widths of at least a few thousand km s^{-1} (for example, Fig. 8). They appear in 10 to 15% of optically-selected QSOs and clearly identify high-velocity winds from the central engines. The precise location of the absorbing gas is unknown, but there is little doubt that it is intrinsic — originating within at least a few tens of parsecs from the QSOs. See recent work by Weymann *et al.* (1991), Barlow *et al.* (1992), Korista *et al.* (1993), Hamann *et al.* (1993), Voit, Weymann & Korista (1993), Murray *et al.* (1995), Arav (1996), Turnshek *et al.* (1997), Brotherton *et al.* (1998b), and the reviews by Turnshek (1988, 1994), Weymann, Turnshek & Christianen (1985) and Weymann (1994, 1997).

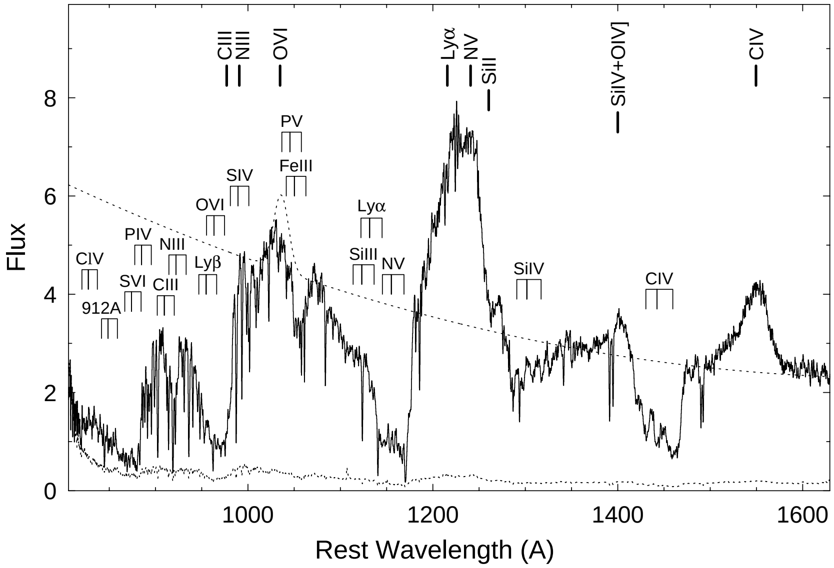

Fig. 8 — Spectrum of the BALQSO PG 1254+047 (emission redshift $z_e = 1.01$) with emission lines labeled across the top and possible BALs marked below at redshifts corresponding to the 3 deepest minima in the CIV trough. Not all of the labeled lines are detected. The smooth dotted curve is a power-law continuum fit extrapolated to short wavelengths (from Hamann 1998).

3.1.2. Narrow Absorption Lines (NALs)

A practical definition of NALs would limit their full widths at half minimum (FWHMs) to less than the velocity separation of important doublets (e.g. <500 km s^{-1} for CIV, <1930 km s^{-1} for SiIV or <960 km s^{-1} for NV), because it is our ability to resolve these doublets that makes their analysis fundamentally different from the BALs (§3.2.2 below).

NALs can form in a variety of locations, ranging from very near QSOs, as in ejecta like the BALs, to unrelated gas or galaxies at cosmological distances (Weymann *et al.* 1979). It is not yet known what fraction of NALs at any velocity shift meet our definition of intrinsic (§1). Several studies have noted a statistical excess of NALs within a few thousand km s^{-1} of the emission redshifts. These are the so-called "associated" or $z_a \approx z_e$ absorbers (with redshifts close to the emission redshift, Weymann *et al.* 1979 and 1981, Young *et al.* 1982, Foltz *et al.* 1986 and 1988, Anderson *et al.* 1987). Their strengths and frequency of occurrence appear to correlate with the QSO luminosities or radio properties, suggesting some physical relationship (also Möller *et al.* 1994, Aldcroft, Bechtold & Elvis 1994, Wills *et al.* 1995, Barthel, Tytler & Vestergaard 1997). These correlations may extend to NALs at blueshifts of 30,000 km s^{-1} or more (Richards & York 1998). Nontheless, we might expect a larger fraction of intrinsic NALs nearer the emission redshift and, if they are ejected from QSOs, they should appear at $z_a < z_e$ rather than $z_a > z_e$.

Several tests have been developed to help identify intrinsic NALs, including 1) time-variable line strengths, 2) multiplet ratios that imply partial line-of-sight coverage of the background light source(s), 3) high gas densities inferred from excited-state absorption lines, and 4) well-resolved line profiles that are smooth and broad compared to both thermal line widths and to the velocity dispersions expected in intervening clouds (e.g. Bahcall, Sargent & Schmidt 1967, Williams *et al.* 1975, Young *et al.* 1982, Barlow & Sargent 1997, Hamann *et al.* 1997b – hereafter H97b, Hamann *et al.* 1997c, Petitjean & Srianand 1999, Ganguly *et al.* 1999, and refs. therein). These criteria might not be definitive individually, but they sometimes appear in combination.

Figure 9 shows a $z_a \approx z_e$ NAL system that is clearly intrinsic based on time-variable line strengths, partial line-of-sight coverage and relatively broad profiles. High metallicities might be another indicator of intrinsic absorption (§3.4 below), but that criterion would bias abundance studies; we would like to determine the intrinsic versus intervening nature independent of the abundances. The other (non-abundance) tests indicate that intrinsic NALs can have velocity shifts out to $\gtrsim$24,000 km s^{-1} and a wide range of FWHMs down to $\lesssim$30 km s^{-1}. See the references above and the reviews of $z_a \approx z_e$ systems by Weymann *et al.* (1981) and Foltz *et al.* (1988).

3.2. General Abundance Analysis

Abundance estimates from absorption lines are, in principle, more straightforward than for emission lines because the absorption strengths are not sensitive to the temperatures or space densities. Moreover, absorption lines yield direct measures of the column densities in different ions. We need only apply appropriate ionization corrections to convert the column densities into relative abundances. For example, the abundance ratio of any two elements a and b can be written,

$$\left[\frac{a}{b}\right] \; = \; \log\left(\frac{N(a_i)}{N(b_j)}\right) \; + \; \log\left(\frac{f(b_j)}{f(a_i)}\right) \; + \; \log\left(\frac{b}{a}\right)_{\odot} \qquad (10)$$

which is identical to Equation 8 except that the N here are the column densities. Once again we define the ionization correction as $IC \equiv \log(f(b_j)/f(a_i))$. Abundance studies would ideally compare lines with similar ionizations to minimize IC and reduce the sensitivity to potentially complex geometries. Unfortunately, the lines available often require significant ionization corrections. In particular, we are often forced to compare highly-ionized metals (such as CIV) to HI (Lyα) to derive the metallicity. We must therefore use ionization models.

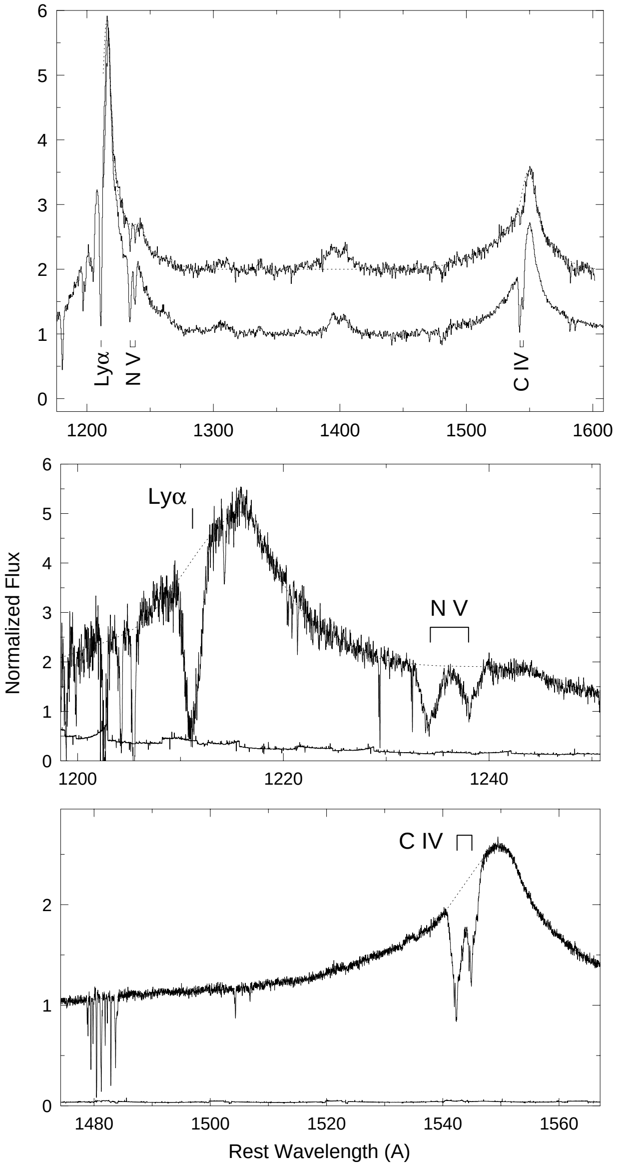

Fig. 9 — Spectra of the $z_a \approx z_e$ absorber in UM675 ($z_e = 2.15$) showing its time-variability in two epochs (top panel) and broad, smooth profiles at higher spectral resolution (9 km s^{-1}, bottom panels, from Hamann *et al.* 1995, 1997b).

The usual assumption is that the gas is photoionized by the QSO continuum flux. Collisional ionization would lead to lower derived metallicities because it creates less HI (and more HII) for a given level of ionization in the metals (cf. Figs. 4 and 5 in Hamann *et al.* 1995, also Turnshek *et al.* 1996). However, collisional ionization has been generally dismissed for BAL regions (BALRs) because 1) it would be energetically hard to maintain, 2) it would produce excessive amounts of line emission (because of the much higher temperatures), and 3) it is hard to reconcile with the observed simultaneous variabilities in BAL troughs across a wide range of velocities (Weymann *et al.* 1985, Junkkarinen *et al.* 1987, Barlow 1993). In contrast, the strong radiative flux known to be present in QSOs provides a natural ionization source. We will assume that photoionization dominates in both BALRs and intrinsic NALRs.

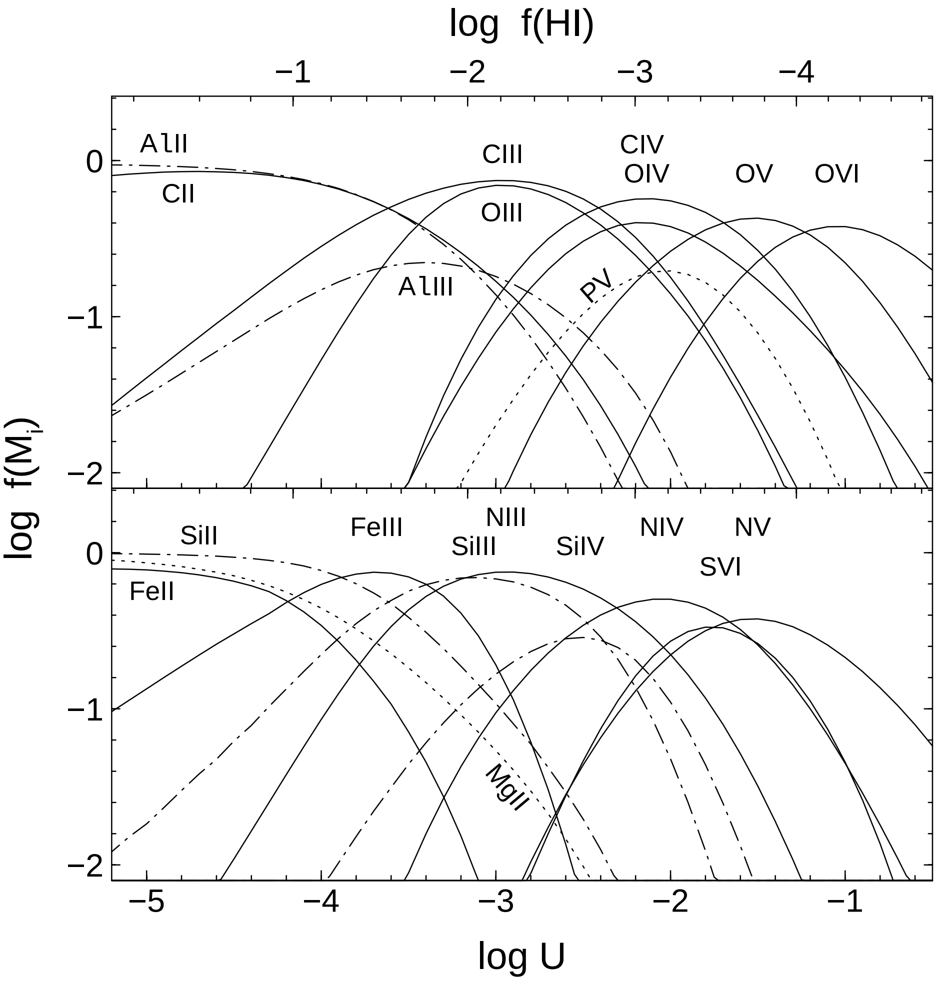

Fig. 10 — Ionization fractions in optically thin clouds photoionized at different U by a power-law spectrum with $\alpha = -1.5$. The HI fraction appears across the top. The curves for the metal ions are labeled above or below their peaks whenever possible. The notation here is HI = H^o, CIV = C^{+3}, etc.

Estimates of IC generally come from plots like Figure 10, which shows the ionization fractions of HI and various metal ions M_i in photoionized clouds (see §2.5 and Ferland *et al.* 1998 for general descriptions of the calculations). Ideally, we would compare column densities in different ions of the same element to obtain abundance-independent constraints on the ionization and thus IC. Otherwise, column densities in different elements can also constrain IC with assumptions about the relative abundances. Note that the results in Figure 10 are not sensitive to the particular abundances used the calculations (in this case solar), so the figure is useful for general abundance/ionization estimates (see Hamann 1997 — hereafter H97). The model clouds are optically thin in the ionizing UV continuum, which means that gradients in the ionization are negligible across the cloud and the ionization fractions do not depend on the total column densities. This simplification appears to be appropriate for most intrinsic absorption line systems (based on their measured column densities), although shielding by many far-UV BALs might affect the ionization structure downstream in BALRs (Korista *et al.* 1996, Turnshek 1997, H97). Also, systems with low-ionization lines like FeII or MgII can be optically thick at the HI Lyman edge (Bergeron & Stasińska 1986, Voit *et al.* 1993, Wampler, Chugai & Petitjean 1995) and may require calculations with specific column densities that match the data.

3.2.1. Ionization Ambiguities

The main theoretical uncertainties involve the shape of the ionizing spectrum, the frequent lack of ionization constraints (too few lines measured), and the possibility of inhomogeneous (multi-zone) absorbing media. H97 addressed these issues by calculating IC values for a wide range of conditions in photoionized clouds. He noted that, whenever there is or might be a multi-zone with a range of ionizations, we can still make conservatively low estimates of the metal-to-hydrogen abundance ratios by assuming each metal line forms where that ion is most favored — that is, at the peak of its ionization fraction $f(M_i)$ in Figure 10. We can also place firm lower limits on the metal-to-hydrogen ratios by adopting the minimum values of IC, which correspond to minima in the $f(\mathrm{HI})/f(\mathrm{M}_i)$ ratios (see also Bergeron & Stasińska 1986). The lower limits are robust, even though they come from 1-zone calculations, because different or additional zones can only mean that larger IC values are appropriate for the data. Figure 11 plots several minimum metal-to-hydrogen ICs for optically thin clouds photoionized by different power-law spectra. The results in this plot simply get added to the logarithmic column density ratios (Eqn. 10) to derive minimum metallicities. Note that some important metal-to-metal ratios also have minimum IC values, such as PV/CIV and FeII/MgII (Hamann 1998, Hamann *et al.* 1999b).

3.2.2. Column Densities and Partial Coverage

The final critical issue is deriving accurate column densities from the absorption troughs. In the simplest case, the line optical depths are related to the observed intensities by,

$$I_v \;=\; I_o \exp\left(-\tau_v\right) \tag{11}$$

where I_v and I_o are the observed and intrinsic (unabsorbed) intensities, respectively, and τ_v is the line optical depth, at each velocity shift v. The column densities follow from the optical depths by,

$$N \;=\; \frac{m_e c}{\pi e^2 f \lambda_o} \int \tau_v \; dv \tag{12}$$

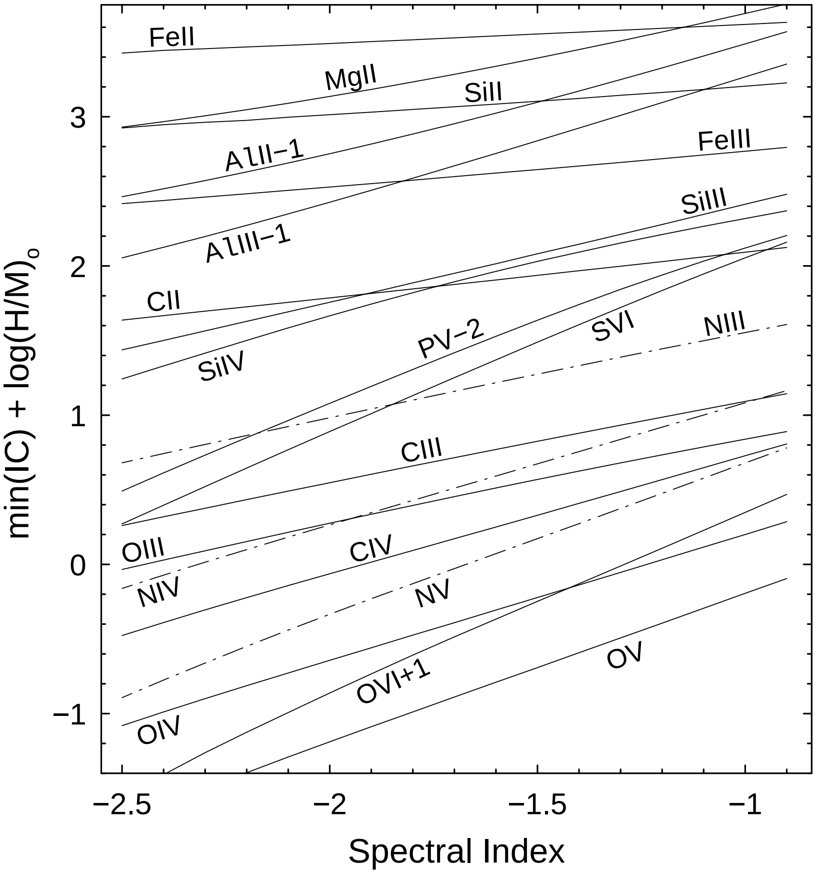

Fig. 11 — Minimum metal ion to HI ionization corrections (IC) normalized to solar abundances (the last two terms in Eqn. 10) are plotted for optically thin clouds photoionized by power-law spectra with different indices (α). The notation is the same as Fig. 10. The curves have been shifted vertically by +1 for OVI, by −2 for PV, and by −1 for AlII and AlIII. The curves for nitrogen ions are dash-dot.

where f is the oscillator strength and λ_o is the laboratory wavelength of the line. Column density derivations can involve line profile fitting or direct integration over the observed profiles (via Eqns. 11 and 12, Junkkarinen *et al.* 1983, Grillmair & Turnshek 1987, Korista *et al.* 1992, Savage & Sembach 1991, Jenkins 1996, Arav *et al.* 1999 — hereafter A99). Very optically thick lines are not useful because the inferred values of τ_v are far too sensitive to uncertainties in I_v. In other cases, the analysis might still be compromised by 1) unresolved absorption-line components or 2) unabsorbed flux that fills in the the bottoms of the observed troughs. If either of these possibilities occurs, the derived optical depths and column densities become lower limits and the derived abundances become incorrect. Errors from the first possibility can always be reduced or avoided by higher resolution spectroscopy.

XXXXXX INSERT FIGURE HERE XXXXXX

Fig. 12 — Schematic showing possible "partial coverage" geometries. Partial line-of-sight coverage occurs when light rays like C, which pass through absorption-line clouds (indicated by filled ellipsoids), are combined with rays like A, B or D, which do not. Ray A represents reflected light from a putative scattering region. Ray B simply misses the absorption-line region. Ray D passes through the nominal absorbing zone but suffers no absorption because the region is porous.

The second possibility, of filled-in absorption troughs, is actually an asset for identifying intrinsic NALs (§3.1). We will refer to this filling-in generally as "partial coverage" of the background emission source. Figure 12 shows several geometries that might produce partial coverage and filled-in troughs[3]. When partial coverage occurs, the observed intensities depend on both the optical depth and the line-of-sight coverage fraction, C_f, at each velocity,

$$I_v \;=\; (1-C_f)\,I_o \,+\, C_f\,I_o\,\exp\left(-\tau_v\right) \tag{13}$$

where $0 \leq C_f \leq 1$ and the first term on the right side is the unabsorbed (or uncovered) contribution. Measured absorption lines can thus be shallow even when the true optical depths are large. In the limit $\tau_v \gg 1$, we have,

$$C_f \;=\; 1-\frac{I_v}{I_o} \tag{14}$$

Outside of that limit, we can compare lines whose true optical depth ratios are fixed by atomic physics, such as the HI Lyman lines or doublets like CIV $\lambda\lambda$1548,1550, SiIV $\lambda\lambda$1394,1403, etc., to determine uniquely both the coverage fractions and the true optical depths across the line profiles (H97b, Barlow & Sargent 1997, A99, Srianand & Shankaranarayanan 1999, Ganguly *et al.* 1999). For example, a little algebra shows that for doublets with true optical depth ratios of ∼2 (as in CIV, SiIV, etc.) the coverage fraction at each absorption velocity is,

$$C_f \;=\; \frac{I_1^2-2I_1+1}{I_2-2I_1+1} \tag{15}$$

where I_1 and I_2 are the observed line intensities, normalized by I_o, at the same velocity in the weaker and stronger line troughs, respectively. The corresponding line optical depths are $\tau_2 = 2\tau_1$ and,

$$\tau_1 \;=\; \ln\left(\frac{C_f}{I_1+C_f-1}\right) \tag{16}$$

It is a major strength of the NALs that we can resolve key multiplet lines and use this analysis to measure the coverage fractions and thus derive reliable column densities and

---

[3] The situation can be potentially more complicated if the absorber itself is a source of emission. The analysis discussed below remains the same, however.

abundances. It is a great weakness of the BALs that this analysis is usually not possible because the lines are blended. We will argue below that BAL studies so far have been seriously compromised by unaccounted for partial-coverage effects.

The only drawback of partial coverage for the NALs is that there might be a range of coverage fractions in multi-zone absorbing media. There is already evidence in some cases for coverage fractions that differ between ions or change with velocity across the line profiles (Barlow & Sargent 1997, Barlow, Hamann & Sargent 1997, H97b). Variations in C_f with velocity can always be dealt with by analyzing limited velocity intervals in the line profiles (see also Arav 1997). But one can imagine complex geometries where ionization-dependent coverage fractions would jeopardize the simple analysis described above, in particular for comparisons between high and low ionization species like CIV and HI. Abundance ratios based on disparate species like these might require specific models of the ionization-dependent coverage. On the other hand, this worst-case scenario is not known to occur, and there is no reason to believe it would lead to generally overestimated metallicities anyway.

3.3. Broad Absorption Line Results

One common characteristic of BAL spectra is that the metallic resonance lines like CIV λ1548,1951, SiIV λ1394,1403, NV λ1239,1243 and OVI λ1032,1038 are typically strong (deep) compared to Lyα (e.g. Fig. 8). This result, and the fact that low-ionization lines like MgII λ2796,2804 and FeII (UV) are usually absent, indicates that the BALR ionization is generally high (Turnshek 1984, Weymann *et al.* 1981,1985). However, quantitative studies of the ionization have repeatedly failed to explain the measured line strengths with solar abundances. These difficulties were first noted by Junkkarinen (1980) and Turnshek (1981, also Weymann & Foltz 1983), who showed that photoionization models with power-law ionizing spectra and solar abundances underpredict the metal ions, especially SiIV, by large factors relative to HI. A straightforward conclusion is that the metallicities are well above solar. Turnshek (1986, 1988) and Turnshek *et al.* (1987) estimated metal abundances (C/H) of 10 to 100 times solar, and provided tentative evidence for some extreme metal-to-metal abundance ratios such as P/C $\gtrsim$ 100 times solar.

Better data in the past ten years have done nothing to change these startling results (e.g. Turnshek *et al.* 1996). The early concerns about unresolved line components (Junkkarinen *et al.* 1987, Kwan 1990) have gone away, thanks to spectroscopy with the Keck 10 m telescope at resolutions ($\sim$7 km s^{-1}) close to the thermal speeds (Barlow & Junkkarinen 1994, Junkkarinen 1998). The previously tentative detections of PV λ1118,1128 absorption, which led to the large P/C abundance estimates, have now been confirmed in two objects by excellent wavelength coincidences, by the predicted weakness of nearby lines like FeIII λ1122, and in one case by the probable presence of PIV λ951 absorption (Junkkarinen *et al.* 1997, Hamann 1998, Fig. 8). The commonality of PV absorption is not yet known (see also Korista *et al.* 1992, Turnshek *et al.* 1996), but its relative strength in just the two cases is surprising because the solar P/C ratio is only $\sim$0.001.

More complex theoretical analyses, considering a range of ionizing spectral shapes or multiple ionization zones, also do not change the main result for metallicities and P/C ratios well above solar (Weymann *et al.* 1985, Turnshek *et al.* 1987, 1996 and 1997, Korista *et al.* 1996). H97 used the analysis in §3.2 to determine how high the abundances must be given the measured column densities and a photoionized BALR. He showed that average BALR column densities require [C/H] and [N/H] > 0 and [Si/H] > 1.0 for any range of ionizations and reasonable spectral shapes. The conservatively low (but not quite minimum) values of IC indicate [C/H] and [N/H] $\gtrsim 1.0$ and [Si/H] $\gtrsim 1.7$. The results for individual BAL systems can be much higher. In PG1254+047 (Fig. 8, Hamann 1998) the inferred minimum abundances are [C/H] and [N/H] $\gtrsim 1.0$, [Si/H] $\gtrsim 1.8$ and [P/C] $\gtrsim 2.2$.

However, we will now argue that all these BAL abundance results are incorrect, because partial coverage effects have led to generally underestimated column densities.

3.3.1. Uncertainties and Conclusions

There is now direct evidence for partial coverage in some BALQSOs based on widely separated lines of the same ion (A99) and resolved doublets in several narrow BALs and BAL components (Telfer *et al.* 1999, Barlow & Junkkarinen 1994, Wampler *et al.* 1995, Korista *et al.* 1992 — confirmed by Junkkarinen 1998). Although most this evidence applies to narrow features, it is noteworthy that there are no counterexamples to our knowledge — where narrow line components associated with BALs indicate complete coverage (also Junkkarinen 1998).

There is also circumstantial evidence for partial coverage in BAL systems. Namely, 1) spectropolarimetry indicates that BAL troughs can be filled in by polarized flux (probably from an extended scattering region) that is not covered by the BALR (Fig. 12, Goodrich & Miller 1995, Cohen *et al.* 1995, Hines & Wills 1995, Schmidt & Hines 1999). 2) Some BAL systems have a wide range of lines with suspiciously similar strengths or flat-bottom troughs that do not reach zero intensity (Arav 1997). 3) Voit *et al.* (1993) made a strong case for low-ionization BALRs being optically thick at the Lyman limit, which implies large optical depths in Lyα, yet the Lyα troughs are not generally black in these systems. 4) The larger column densities that follow assuming partial coverage and saturated BALs ($N_H \gtrsim 10^{22}$ cm^{-2}, Hamann 1998) are consistent with the large absorbing columns inferred from X-ray observations of BALQSOs (Green & Mathur 1996, Green *et al.* 1997, Gallagher *et al.* 1999).

More indirect evidence comes from the abundance results themselves. Voit (1997) noted that the derived overabundances tend to be greater for rare elements like P than for common elements like C. This is precisely what would occur if line saturation is not taken into account. The surprising detections of PV might actually be a signature of line saturation (and partial coverage) in strong lines like CIV, rather than extreme abundances (Hamann 1998). This assertion is supported by the one known NAL system with PV $\lambda\lambda$1118,1128 absorption, where the doublet ratios in CIV, NV and SiIV clearly indicate $\tau \gg 1$ (Barlow *et al.* 1997, Barlow 1998).

We conclude that BAL column densities have been generally underestimated and the true BALR abundances are not known. Observed differences between BAL profiles that resemble simple optical depth effects are probably caused by a mixture of ionization, coverage fraction and optical depth differences in complex, multi-zone BALRs. This conclusion paints a grim picture for BAL abundance work, but it might still be possible to derive accurate column densities and therefore abundances for some BALQSOs or some portions of BAL profiles (Wampler *et al.* 1995, Turnshek 1997, A99). Most needed are spectra at shorter rest-frame wavelengths to measure widely separated lines of the same ion and thereby diagnose the coverage fractions and true optical depths (§3.2.2, Arav 1997, A99).

3.4. Narrow Absorption Line Results

In contrast to the BALs, intrinsic NALs might be the best abundance probes we have for QSO environments. Resolved measurements of NAL multiplets allow us to measure both the coverage fractions and true column densities (§3.2.2). The NALs also allow separate measurements of important lines that are often blended in BAL systems, such as NV λ1239,1243–Lyα, OVI λ1032,1038–Lyβ and many others. We therefore have potentially many more constraints on both the ionization and abundances.

Early NAL studies did not have the quality of data needed to derive column densties and abundances, but several groups noted a tendency for larger NV/CIV line strength ratios in $z_a \approx z_e$ systems compared to $z_a \ll z_e$ (Weymann *et al.* 1981, Hartquist & Snijders 1982, Bergeron & Kunth 1983, Morris *et al.* 1986, Bergeron & Boissé 1986). This trend is probably not due simply to higher ionization in $z_a \approx z_e$ absorbers, because recent studies show that $z_a \ll z_e$ systems typically have strong OVI lines and therefore considerable high-ionization gas; NV appears to be weak relative to both CIV and OVI at $z_a \ll z_e$ (Lu & Savage 1993, Bergeron *et al.* 1994, Burles & Tytler 1996, Kirkman & Tytler 1997, Savage, Tripp & Lu 1998). The lower NV/OVI and NV/CIV line ratios at $z_a \ll z_e$ could be caused by an underabundance of nitrogen (relative to solar ratios) in metal-poor intervening gas (Bergeron *et al.* 1994, Hamann *et al.* 1997d, Kirkman & Tytler 1997). This would be the classic abundance pattern involving secondary nitrogen (Vila-Costas & Edmunds 1993). Relatively higher N abundances and thus stronger NV absorption lines should occur naturally in metal-rich environments near QSOs (see §§6–7 below).

The first explicit estimates of $z_a \approx z_e$ metallicities were by Wampler *et al.* (1993), Möller *et al.* (1994), Petitjean *et al.* (1994) and Savaglio *et al.* (1994) for QSOs at redshifts of roughly 2 to 4. These studies found that $z_a \approx z_e$ systems often have $Z \gtrsim \mathrm{Z}_\odot$, which is at least an order of magnitude larger than the $z_a \ll z_e$ systems measured in the same data. Several of the metal-rich $z_a \approx z_e$ systems have doublet ratios implying partial coverage and thus, very likely, an intrinsic origin (Wampler *et al.* 1993, Petitjean *et al.* 1994). The location of the other $z_a \approx z_e$ absorbers is not known, but Petitjean *et al.* (1994) noted a marked change from [C/H] $\lesssim -1$ to [C/H] $\gtrsim 0$ at a blueshift of $\sim$15,000 km s^{-1} relative to the emission lines. If high abundances occur only in intrinsic systems, then these results suggest that most $z_a \approx z_e$ NALs are intrinsic (also Möller *et al.* 1994).

More recent studies support these findings. Petitjean & Srianand (1999) measured $Z \gtrsim \mathrm{Z}_\odot$ and [N/C] > 0 in an intrinsic (partial coverage) $z_a \approx z_e$ absorber. For $z_a \approx z_e$ systems of unknown origin, Savage *et al.* (1998) estimated roughly solar metallicities and Tripp *et al.* (1997) obtained [N/C] $\gtrsim 0.1$ and, very conservatively, [C/H] $\gtrsim -0.8$. (The lower limit on [C/H] for the latter system is -0.2 when more likely ionizing spectral shapes are used in the calculations.) Savaglio *et al.* (1997) revised the metallicities downward slightly from their 1994 paper to $-1 < \mathrm{[C/H]} < 0$, based on better data. Those systems are of special interest because of their high redshift ($z_a \approx 4.1$). Wampler *et al.* (1996) estimated $Z \sim 2\ \mathrm{Z}_\odot$ (based on a tentative detection of OI λ1303) for the only other $z_a \approx z_e$ systems studied so far at $z > 4$.

H97, H97b and Hamann *et al.* (1995, 1997e, 1999b) used the analysis outlined in §3.2 to determine metallicities or establish lower limits for several $z_a \approx z_e$ systems, including some mentioned above and some that are clearly intrinsic by the indicators in §3.1. The results generally confirm the previous estimates and show further that, even when there are no constraints on the ionization (for example, when only Lyα and CIV lines are measured), the column densities can still require $Z \gtrsim \mathrm{Z}_\odot$. A quick survey of those results suggests that bona fide intrinsic systems, and most others with $Z \gtrsim \mathrm{Z}_\odot$, have $\mathrm{[N/C]} \gtrsim 0.0$.

3.4.1. Uncertainties and Conclusions

Most of the studies mentioned above would benefit from better data (higher signal-to-noise ratios and higher spectral resolutions) and more ionization constraints (wider wavelength coverage), but the frequent result for $Z \gtrsim \mathrm{Z}_\odot$ is convincing. Unlike the BALs, there are no obvious systematic effects that might lead to higher abundance estimates for $z_a \approx z_e$ systems compared to $z_a \ll z_e$. The possibility of ionization-dependent coverage fractions presents an uncertainty for those systems with partial coverage, but we do not expect that to cause systematic overestimates of the metallicities (§3.2.2). We conclude that many $z_a \approx z_e$ NALs and, more importantly, all of the "confirmed" intrinsic systems, have $Z \gtrsim 0.5\mathrm{Z}_\odot$ and usually $Z \gtrsim \mathrm{Z}_\odot$. The upper limits on Z are uncertain. The largest estimate for a well-measured system is $Z \sim 10\ \mathrm{Z}_\odot$ (Petitjean *et al.* 1994), but those data are also consistent with metallicities as low as solar because of ionization uncertainties (H97). There are mixed and confusing reports in the literature regarding metal-to-metal abundance ratios, most notably N/C. In contrast to Franceschini & Gratton (1997), we find no tendency for sub-solar N/C in $z_a \approx z_e$ systems. In fact, there is the general trend for stronger NV absorption at $z_a \approx z_e$ compared to $z_a \ll z_e$ systems, and the most reliable abundance data suggest solar or higher N/C ratios whenever $Z \gtrsim \mathrm{Z}_\odot$.

The only serious problem is in interpreting the abundance results for systems of unknown origin. High metallicities might correlate strongly with absorption near QSOs, but the metallicities cannot define the absorber's location. For example, Tripp *et al.* (1996) estimated $Z \gtrsim \mathrm{Z}_\odot$ and $\mathrm{[N/C]} \gtrsim 0$ for a $z_a \approx z_e$ system where the lack of excited-state absorption in CII* λ1336 (compared the measured CII λ1335) implies that the density is low, $\lesssim$7 cm^{-3}, and thus the distance from the QSO is large, $\gtrsim$300 kpc. (The relationship between density and distance follows from the flux requirements for photoionization, §2.5.1.) Super-solar metallicities at these large distances are surprising. At $\gtrsim$300 kpc from the QSO, we might have expected very low intergalactic or halo-like abundances. The solution might be that the absorbing gas was enriched much nearer the QSO and then ejected (Tripp *et al.* 1996).

Unfortunately, the excited-state lines used for density and distance estimates are not generally available for $z_a \approx z_e$ systems (because they have low ionization energies, e.g. CII* and SiII*). Of the six $z_a \approx z_e$ absorbers known to be far ($\gtrsim$10 kpc) from QSOs based on these indicators, three of them clearly have $z_a > z_e$ and are probably not intrinsic for that reason (Williams *et al.* 1975, Williams & Weymann 1976, Sargent *et al.* 1982, Morris *et al.* 1986, Barlow *et al.* 1997). Only one has a metallicity estimate — the system with $Z \gtrsim Z_\odot$ at $\gtrsim$300 kpc distance studied by Tripp *et al.* (1996).

4. General Abundance Summary

The main abundance results are as follows.

1) There is a growing consensus from the BELs and NALs for $Z \gtrsim Z_\odot$ in QSOs out to $z > 4$. The upper limits on the metallicities are not well known, but none of the data require $Z > 10\ Z_\odot$. Solar to a few times solar appears to be typical. Based on very limited data, there is no evidence for a decline at the highest redshifts.

2) A trend in the NV/HeII and NV/CIV BEL ratios suggests that the metallicities are generally higher in more luminous QSOs.

3) The BELs and NALs both suggest that the relative nitrogen abundance (e.g. N/C and N/O) is typically solar or higher. We will argue below (§6) that this result corroborates the evidence for $Z \gtrsim Z_\odot$ (because of the likely secondary origin of nitrogen at these metallicities).

4) There is tentative evidence for super-solar Fe/Mg abundances out to $z > 4$ based on the FeII/MgII BEL strengths. Again, based on limited data, there is no evidence for a decline in this ratio at the highest redshifts.

5) The extremely high metallicities and large P/C ratios derived so far from the BALs are probably incorrect. In further support of that conclusion, we note that BELR simulations using the nominally derived BAL abundances (including large enhancements in P and other odd-numbered elements like Al, Shields 1996) are inconsistent with observed BEL spectra (based on unpublished work in collaboration with G. Shields).

5. Enrichment Scenarios

Several scenarios have been proposed for the production of heavy elements near QSOs, including 1) the normal evolution of stellar populations in galactic nuclei (Hamann & Ferland 1992, HF93b), 2) central star clusters with enhanced supernova (and perhaps nova) rates due to mass accreted onto stars as they plunge through QSO accretion disks (Artimowitz, Lin & Wampler 1993), 3) star formation inside QSO accretion disks (Silk & Rees 1998, Collin 1998), and 4) nucleosynthesis without stars inside accretion disks (Jin, Arnett & Chakrabarti 1989, Kundt 1996).

5.1. Occam's Razor: The Case for Normal Galactic Chemical Evolution

The first scenario listed above, for normal galactic chemical evolution, is most compelling because 1) it is the only one of these processes known to occur and 2) it is sufficient to explain the QSO data. In particular, the stars in the centers of massive galaxies today are (mostly) old and metal rich (Bica, Arimoto & Alloin 1988, Bica, Alloin & Schmidt 1990, Gorgas, Efstathiou & Aragón Salamanca 1990, Bruzual *et al.* 1997, Vazdekis *et al.* 1997, Jablonka, Alloin & Bica 1992, Jablonka, Martin & Arimoto 1996, Feltzing & Gilmore 1998, Worthy, Faber & Gonzalez 1992, Kuntschner & Davies 1997, Sansom & Proctor 1998, Ortolani *et al.* 1996, Sil'chenko, Burenkov & Vlasyuk 1998, Idiart, de Freitas Pacheco, & Costa 1996, Fisher, Franx & Illingworth 1995, Bressan, Chiosi & Tantalo 1996). The exact ages are uncertain, but there is growing evidence for most of the star formation in massive spheroids (ellipticals and the bulges of large spiral galaxies) occurring at redshifts $z \gtrsim 2$–3, especially (but not only) for galaxies in clusters (see also Renzini 1998,1997, Bernardi *et al.* 1998, Bruzual & Magris 1997, Ellis *et al.* 1997, Tantalo, Chiosi & Bressan 1998, Ivison *et al.* 1998, Kodama & Arimoto 1997, Ziegler & Bender 1997, Kauffmann 1996, Van Dokkum *et al.* 1998, Mushotzky & Loewenstein 1997 Spinrad *et al.* 1997, Stanford *et al.* 1998, Heap *et al.* 1998, Barger *et al.* 1998a,b). The star-forming (Lyman-break or Lyα-emission) objects measured directly at $z \gtrsim 3$ might be galactic or proto-galactic nuclei in the throes of rapid evolution (Friaca & Terlevich 1999, Baugh *et al.* 1998, Steidel *et al.* 1998 and 1999, Connolly *et al.* 1997, Lowenthal *et al.* 1997, Trager *et al.* 1997, Hu, Cowie & McMahon 1998, Franx *et al.* 1997, Madau *et al.* 1996, Giavalisco, Steidel & Machetto 1996). These objects are more numerous than QSOs and some have been measured at $z > 5$ (Dey *et al.* 1998, Hu *et al.* 1998, Weymann *et al.* 1998), beyond the highest known QSO redshift of $z \approx 5.0$ (Sloan Digital Sky Survey press release 1998). On the theoretical side, recent cosmic-structure simulations show that proto-galactic condensations can form stars and reach solar or higher metallicities at $z \gtrsim 6$ (Gnedin & Ostriker 1997). Quasars might form in the most massive and most dense of these early-epoch star-forming environments (Turner 1991, Loeb 1993, Haehnelt & Rees 1993, Miralda-Escude & Rees 1997, Haehnelt *et al.* 1998, Spaans & Carollo 1997). They might also form preferentially in globally dense cluster environments, based on the higher detection rates of star-forming galaxies near high-z QSOs (Djorgovski 1998).

The gas in these environments might have been long ago ejected via galactic winds, consumed by central black holes or diluted by subsequent infall, but its signature remains in the old stars today. The mean stellar metallicities[4] in the cores of massive low-redshift galaxies are typically $\langle Z_{stars} \rangle \sim 1$–3 Z$_\odot$ (see refs. listed above). Individual stars are distributed about the mean with metallicities reflecting the gas-phase abundance at the time of their formation. If the interstellar gas is well-mixed and the abundances grow monotonically (as expected in simple enrichment schemes, §6), the gas-phase metallicity, Z_{gas}, will always exceed $\langle Z_{stars} \rangle$. Only the most recently formed stars will have metallicities as high as the gas. Therefore, the most metal-rich stars today should reveal the gas-phase abundances near the end of the last major star-forming epoch.

In the bulge of our own Galaxy, the nominal value of $\langle Z_{stars} \rangle$ is 1 Z$_\odot$ and the tail of the distribution reaches $Z_{stars} \gtrsim 3$ Z$_\odot$, with even higher values obtaining near the Galactic center (Rich 1988 and 1990, Geisler & Friel 1992, McWilliam & Rich 1994, Minniti *et al.*

---

[4] It is worth noting here that, because of a significant time-delay in the iron enrichment, O/H and Mg/H are better measures of the overall "metallicity" than Fe/H (see §6 and Wheeler *et al.* 1989).

1995, Tiede, Frogel & Terndrup 1995, Terndrup, Sadler & Rich 1995, Idiart *et al.* 1996, Castro *et al.* 1996, Bruzual *et al.* 1997). The gas-phase metallicity should therefore have been $Z_{gas} \gtrsim 3$ Z$_\odot$ after most of the Bulge star formation occurred. Simple chemical evolution models indicate more generally that Z_{gas} should be ~2 to 3 times $\langle Z_{stars} \rangle$ in spheroidal systems like galactic nuclei (Searle & Zinn 1978, Tinsley 1980, Rich 1990, Edmunds 1992, de Fretas Pacheco 1996). Thus the observations of $\langle Z_{stars} \rangle \sim$ 1–3 Z$_\odot$ suggest that gas with $Z_{gas} \sim$ 2–9 Z$_\odot$ once existed in these environments.

We might therefore expect to find $2 \lesssim Z \lesssim 9$ Z$_\odot$ in QSOs, as long as 1) most of the local star formation occurred before the QSOs "turned on" or became observable and 2) the metal-rich gas produced by that star formation was not substantially diluted or ejected. These expectations are consistent with the abundance estimates reported above (§4). More exotic enrichment schemes are therefore not needed to explain the QSO data.

6. More Insights from Galactic Chemical Evolution

If we assume that QSO environments were indeed enriched by normal stellar populations, then we can use the results from galactic abundance and chemical evolution studies to interpret the QSO data. Here we describe some relevant galactic results (see Wheeler, Sneden & Truran 1989 for a general review).

6.1. The Galactic Mass-Metallicity Relation

One important result from galaxy studies is the well-known mass–metallicity relationship among ellipticals and spiral bulges (Faber 1973, Faber *et al.* 1989, Bender, Burstein & Faber 1993, Zaritsky, Kennicutt & Huchra 1994, Jablonka *et al.* 1996, Coziol *et al.* 1997). This relationship is attributed to the action of galactic winds; massive galaxies reach higher metallicities because they have deeper gravitational potentials and are better able to retain their gas against the building thermal pressures from supernovae (Larson 1974, Arimoto & Yoshii 1987, Franx & Illingworth 1990). Low-mass systems eject their gas before high Z's are attained. Quasar metallicities should be similarly tied to the gravitational binding energy of the local star-forming regions and, perhaps, to the total masses of their host galaxies (§7.1 below).

6.2. Specific Abundance Predictions

Another key result is the abundance behaviors of N and Fe relative to the α elements such as O, Mg and Si. HF93b constructed 1-zone infall models of galactic chemical evolution to illustrate these behaviors in different environments. Figure 13 plots the results for two scenarios at opposite extremes. Both use the same nucleosynthetic yields, but the "Giant Elliptical" model has much faster evolution rates and a flatter IMF (more favorable to high-mass stars) compared to the "Solar Neighborhood" (or spiral disk) case. The Giant Elliptical evolves passively (without further star formation) after ~1 Gyr because the gas is essentially exhausted. The parameters used in these calculations were based on standard galactic infall models (e.g. Arimoto & Yoshii 1987, Matteucci & Tornambé 1987, Matteucci & Francois 1989, Matteucci & Brocato 1990, Köppen & Arimoto 1990). However, the results are only illustrative and not intended to match entire galaxies. For example, evolution like the Giant Elliptical model might occur in just the central cores of extreme high-mass galaxies (cf. Friaca & Terlevich 1998).

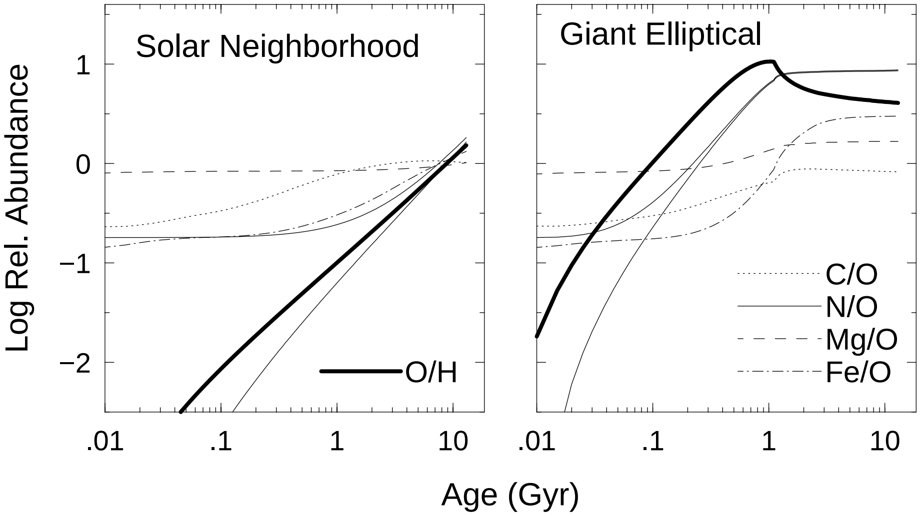

Fig. 13 — Logarithmic gas-phase abundance ratios normalized to solar for the two evolution models discussed in §6.2 (adapted from HF93b). Two scenarios for the N enrichment are shown (thin solid lines); one with secondary only and the other with secondary+primary (causing a plateau in N/O at low Z).

6.3. Fe/α as a Clock

At early times the abundance evolution is controlled by short-lived massive stars, mainly via type II supernovae (SN II's). The α elements, such as O and Mg, come almost exclusively from these objects, but Fe has a large delayed contribution from type Ia supernovae (SN Ia's) — whose precursors are believed to be intermediate mass stars in close binaries (Branch 1998). The predicted time delay is roughly 1 Gyr based on the IMF-weighted stellar lifetimes (Fig. 13, Greggio & Renzini 1983, Matteucci & Greggio 1986). The actual delay is uncertain, but recent estimates are in the range ~0.3 to 3 Gyr (Matteucci 1994, Yoshii, Tsujimoto & Nomoto 1996, Yoshii *et al.* 1998). Because this delay does not depend on any of the global evolution time scales (e.g. the star formation rate, etc.), Fe/α can serve as an absolute "clock" for constraining the ages of star-forming environments (Tinsley 1979, Thomas, Greggio & Bender 1998).

Observations of metal-poor Galactic stars suggest that the baseline value of [Fe/α] due to SN II's alone is nominally −0.7 to −0.4 (Israelian, Garcia & Rebolo 1998, Nissen *et al.* 1994, King 1993, Gratton 1991, Magain 1989, Barbuy 1988, also de Freitas Pacheco 1996), which is slightly larger than the prediction in Figure 13. The subsequent increase caused by SN Ia's is a factor of a few or more. Note that the increase in Fe/α should be larger in rapidly-evolving spheroidal systems because 1) by the time their SN Ia's "turn on," there is relatively little gas left and each SN Ia has a greater effect, also 2) their rapid early star formation means that the SN Ia's occurring later are more nearly synchronized. The net result can be substantially super-solar Fe/α in the gas (even though Fe/α is sub-solar in most stars).

6.4. Nitrogen Abundances

Nitrogen also exhibits a delayed enhancement, although not on a fixed time scale like Fe/α. Nitrogen's selective behavior is due to secondary CNO nucleosynthesis, where N forms out of pre-existing C and O. Studies of galactic HII regions indicate that secondary processing dominates at metallicities above $\sim$0.2 $Z_\odot$, resulting in N/O scaling like O/H (or N $\propto Z^2$) in that regime. At lower metallicities, primary N can be more important based on an observed plateau in [N/O] at roughly -0.7 (see Tinsley 1980, Vila-Costas & Edmunds 1993, Thurston, Edmunds & Henry 1996, Van Zee, Skillman & Salzer 1998, Kobulnicky & Skillman 1998, Thuan, Izotov & Lipovetsky 1995, Izotov & Thuan 1999, but see also Garnett 1990, Lu *et al.* 1998). The models in Figure 13 show two N/O behaviors, for secondary only and secondary+primary, where the latter has a low-Z plateau forced to match the HII region data. Notice that the secondary growth in N/O can be shifted down considerably from the simple theoretical relation [N/O] = [O/H] because of the delays related to stellar lifetimes. We therefore have a strong prediction, based on both observations and these simulations, that measured values of [N/O] $\gtrsim 0$ imply $Z \gtrsim Z_\odot$ — especially in fast-evolving spheroidal systems. This prediction was exploited above in the analysis of QSO BELs (§2.6, Shields 1976).

7. Implications of QSO Abundances

7.1. High-Redshift Star Formation

We can conclude from the previous sections that QSOs are associated with vigorous star formation, consistent with the early-epoch evolution of massive galactic nuclei or dense proto-galactic clumps (§5). However, QSO abundances provide new constraints. For example, the general result for $Z \gtrsim Z_\odot$ suggests that most of the enrichment and local star formation occurs before QSOs "turn on" or become observable. The enrichment times can be so short in principle (Fig. 13, HF93b) that the star formation might also be coeval with QSO formation. In any event, the enrichment times cannot be much longer that $\sim$1 Gyr for at least the highest redshift objects (depending on the cosmology, Fig. 1).

If the QSO metallicities representative of a well-mixed interstellar medium, we can conclude further that the star formation was extensive. That is, a significant fraction of the initial gas must be converted into stars and stellar remnants to achieve $Z_{gas} \gtrsim Z_\odot$. The exact fraction depends on the IMF. A solar neighborhood IMF (Scalo 1990, as in the Solar Neighborhood model of §6) would lead to mass fractions in gas of only $\lesssim$15% at $Z \sim Z_\odot$, and would not be able to produce Z_{gas} above a few $Z_\odot$ at all. Flatter IMFs (favoring massive stars) could reach $Z_{gas} \gtrsim Z_\odot$ while consuming less of the gas. For example, the gas fraction corresponding to $Z_{gas} \sim Z_\odot$ in the Giant Elliptical model of §6.2 is nearly 70%.

Figure 7 in §2.6.3 illustrates the main star formation characteristics required by the QSO data. The solid curves on the right-hand side of that figure show theoretical BEL ratios from photoionization simulations that use nominal BELR parameters and abundances from the two chemical evolution models in Figure 13 (see HF93b for more details). The evolution is assumed to begin with the Big Bang and the conversion of time into redshift assumes a cosmology with $H_o = 65$ km s^{-1} Mpc^{-1}, $\Omega_M = 1$ and $\Omega_\Lambda = 0$ (Fig. 1). The main results are that the Solar Neighborhood evolution is too slow and, in any case, does not reach high enough metallicities or nitrogen enhancements to match most of the high-redshift QSOs. Much shorter time scales and usually higher metallicities, as in the Giant Elliptical simulation, are needed.

A trend in the NV BELs suggests further that the metallicities are typically higher in more luminous QSOs (§2.6.3). That result needs confirmation, but it could result naturally from a mass–metallicity relationship among QSO host galaxies that is similar (or identical to) the well-known relation in low-redshift galaxies (§6, HF93b). By analogy with the galactic relation, the most luminous and metal-rich QSOs might reside in the most dense or massive host environments. This situation would be consistent with studies showing that QSO luminosities, QSO masses, and central black hole masses in galactic nuclei all appear to correlate with the mass of the surrounding galaxies (McLeod *et al.* 1999, McLeod & Rieke 1995, Bahcall *et al.* 1997, Magorrian *et al.* 1998, Laor 1998, also Haehnelt & Rees 1993). A direct application of the galactic mass-metallicity relation suggests that metal-rich QSOs reside in galaxies (or proto-galaxies) that are minimally as massive (or as tightly bound) as our own Milky Way.

7.2. Fe/α: Timescales and Cosmology

One of the most interesting predictions from galactic studies (§6) is that Fe/α ratios in QSOs might constrain the epoch of their first star formation and perhaps the cosmology. In particular, large Fe/α ratios (solar or higher) would suggest that the local stellar populations are at least ∼1 Gyr old. At the highest QSO redshifts ($z \sim 5$), this age constraint would push the epoch of first star formation beyond the limits of current direct observation, to $z > 6$ (Fig. 1). The ∼1 Gyr constraint would also be difficult to reconcile with $\Omega_M \approx 1$ in Big Bang cosmologies. Conversely, measurements of low Fe/α would suggest that the local stellar populations are younger than ∼1 Gyr (although we could not rule out the possibility that only SN II's contributed to the enrichment for some reason). Some BEL studies have already suggested that Fe/α is above solar in $z > 4$ QSOs (§2.6.4).

7.3. Comparisons to Other Results

Quasar abundances should be viewed in the context of other measures of the metallicity and star formation at high redshifts. Damped-Lyα absorbers in QSO spectra, which probe lines of sight through large intervening galaxies (probably spiral disks, Prochaska & Wolfe 1998), have mean (gas-phase) metallicities of order 0.05 $\mathrm{Z}_\odot$ at $z \gtrsim 2$ (Lu *et al.* 1996, Pettini *et al.* 1997, Lu, Sargent & Barlow 1998, Prochaska & Wolfe 1999). The Lyα forest absorbers, which presumably probe much more extended and tenuous inter-galactic structures (Rauch 1998), typically have metalicities <0.01 $Z_\odot$ at high redshifts (Rauch, Haehnelt & Steinmetz 1997, Songalia & Cowie 1996, Tytler *et al.* 1995). The much higher metal abundances near QSOs are consistent with the rapid and more extensive evolution expected in dense environments (Gnedin & Ostriker 1997). Perhaps this evolution is similar to that occurring in the many star-forming objects that are now measured directly at redshifts comparable to, and greater than, the QSOs (see refs. in §5.1).

The detections of strong dust and molecular gas emissions from QSOs support the evidence from their high abundances that considerable local star formation preceded the QSO epoch. The dust and molecules, presumably manufactured by stars, appear even in QSOs at $z \gtrsim 4$ (Isaac *et al.* 1994, Omont *et al.* 1996, Guilloteau *et al.* 1997).

8. Future Prospects

We now have the observational and theoretical abilities to test and dramatically extend all of the QSO abundance work discussed above. The most pressing needs are to 1) develop more independent abundance diagnostics, and 2) obtain more and better data to compare diagnostics in large QSO samples — spanning a range of redshifts, luminosities, radio properties, etc. Absorption line studies will benefit generally from higher spectral resolutions and wider wavelength coverage, providing more accurate column densities and more numerous constraints on the coverage fractions, ionizations and abundances (§3). BEL studies should include more of the weaker lines, such as OVI λ1034, CIII λ977, NIII λ991 and the intercombination lines, whenever possible (§2). Theoretical analysis of the FeII/MgII emission ratios, in particular, is needed to test the tentative conclusion for high Fe/Mg abundances. This and other BEL results should be tested further by examining the same lines (or same elements) in intrinsic NAL systems. The steady improvement in our observational capabilities at all wavelengths will provide many more diagnostic opportunities.

Below are some specific issues that new studies might address.

1) More data at high redshifts will constrain better the epoch and extent of early star formation associated with QSOs.

2) Reliable measurements of Fe/α will further constrain the epoch of first star formation and, perhaps, the cosmology via the ~1 Gyr enrichment clock.

3) Better estimates of the metal-to-metal ratios generally will reveal more specifics of the star formation histories via comparisons to well-studied galactic environments and theoretical nucleosynthetic yields.

4) Abundances for QSOs spanning a wide range of luminosities and redshifts will isolate any evolutionary (redshift) trends and test the tentative luminosity–Z relationship. This relationship might prove to be a useful indicator of the total masses or densities of the local stellar populations by analogy with the mass–Z trend in nearby galaxies.

5) The range of QSO metallicities at a given redshift and luminosity will help constrain the extent of star formation occurring before QSOs turn on or become observable. Are there any low metallicity QSOs?

6) Combining the QSO abundances with direct imaging studies of their host galaxies

should test ideas about the chemical enrichment and help us interpret data at the highest redshifts where direct imaging is (so far) not possible. For example, are QSOs in large galaxies (e.g. giant ellipticals) more metal-rich than others?

7) Correlations between the abundances and other properties of QSOs, such as radio-loudness or UV–X-ray continuum shape, might reveal new environmental factors in the enrichment or systematic uncertainties in our abundance derivations.

8) Observations with wide wavelength coverage would allow us to compare abundances derived from the narrow emission lines (in the rest-frame optical) to BEL and NAL data in the same objects. These diverse diagnostics might provide crude abundance maps of QSO host galaxies.

9) How do QSO abundances compare to their low-redshift counterparts, the Seyfert galaxies and active galactic nuclei (AGNs)? Low-redshift metallicities might be less than the QSOs due to recent mergers or gaseous infall.

ACKNOWLEDGEMENTS

We are grateful to G Burbidge for his patience and encouragement. We also thank KT Korista and JC Shields for helpful comments on this manuscript, and TA Barlow, N Arav and VT Junkkarinen for useful discussions. GF thanks the Canadian Institute for Theoretical Astrophysics for their hospitality during a sabbatical year, and acknowledges support from the Natural Science and Engineering Research Council of Canada through CITA. The work of FH was supported by NASA grant NAG 5-3234. Research in nebular astrophysics at the University of Kentucky is supported by the NSF through grant 96-17083 and by NASA through its ATP (award NAG 5-4235) and LTSA programs.

9. Literature Cited

Aldcroft TL, bechtold J, Elvis M. 1994, *Ap. J. Suppl.* 93, 1

Anderson SF, Weymann RJ, Foltz CB, Chaffee FH. 1987, *Astron. J.* 94, 278

Arav N. 1996, *Ap. J.* 465, 617

Arav N. 1997, in Mass Ejection From AGN, eds. R Weymann, I Shlosman, N Arav, ASP Conf. Series, 128, 208

Arav N, Barlow TA, Laor A, Sargent WLW, Blandford RD. 1998, *MNRAS* 297, 990

Arav N, Korista KT, de Kool M, Junkkarinen VT, Begelman MC. 1999, *Ap. J.* in press (A99)

Aretxaga I, Terlevich RJ, Boyle BJ. 1998, *MNRAS* 296, 643

Arimoto N Yoshii Y. 1987, *Astron. Astrophys.* 173, 23

Artymowicz P, Lin DNC, Wampler EJ. 1993, *Ap. J.* 409, 592

Bahcall JN, Kirhakos S, Saxe DH, Schneider DP. 1997, *Ap. J.* 479, 642

Bahcall JN, Sargent WLW, Schmidt M. 1967, *Ap. J.* 149, L11

Baldwin JA. 1977a, *MNRAS* 178, 67P

Baldwin JA. 1977b, *Ap. J.* 214, 679

Baldwin JA, & Netzer H. 1978, *Ap. J.* 226, 1

Baldwin JA, Ferland GJ, Korista KT, Carswell RF, Hamann F, *et al.* 1996, *Ap. J.* 461, 664

Baldwin JA, Ferland GJ, Korista KT, Verner D. 1995, *Ap. J.* 455, L119

Barbuy B. 1988, *Astron. Astrophys.* 191, 121

Barger AA, Aragon-Salamanca A, Smail I, Ellis RS, Couch WJ, *et al.* 1998a, *Ap. J.* 501, 522

Barger AA, Cowie LL, Trentham N, Fulton E, Hu EM, *et al.* 1998b, preprint (astro-ph/9809299)

Barlow TA. 1993, Ph.D. Dissertation, University of California – San Diego

Barlow TA. 1998, private comm.

Barlow TA, Hamann F, Sargent WLW. 1997, in Mass Ejection From AGN, eds. R Weymann, I Shlosman, N Arav, ASP Conf. Series, 128, 13

Barlow TA, Junkkarinen VT. 1994, BAAS, 26, 1339

Barlow TA, Junkkarinen VT, Burbidge EM, Weymann RJ, Morris SL, *et al.* 1992, *Ap. J.* 397, 81

Barlow TA, Sargent WLW. 1997, *Astron. J.* 113, 136

Barthel PD, Tytler DR, Vestergaard M. 1997, in Mass Ejection From AGN, eds. R Weymann, I Shlosman, N Arav, ASP Conf. Series, 128, 48

Baugh CM, Cole S, Frenk CS, Lacey CG. 1998, *Ap. J.* 498, 504

Bender R, Burstein D, Faber SM. 1993, *Ap. J.* 411, 153

Bergeron J, Boissé P. 1986, *Astron. Astrophys.* 168, 6

Bergeron J, Kunth D. 1983, *MNRAS* 205, 1053

Bergeron J, Petitjean P, Sargent WLW, Bahcall JN, Boksenberg A, *et al.* 1994, *Ap. J.* 436, 33

Bergeron J Stasińska G. 1986, *Astron. Astrophys.* 169, 1

Bernardi M, Renzini A, da Costa LN, Wegner G, Victoria M, *et al.* 1998, preprint (astro-ph/9810066)

Bica E, Alloin D, Schmidt AA. 1990, *Astron. Astrophys.* 228, 23

Bica E, Arimoto N, Alloin D. 1988, *Astron. Astrophys.* 202, 8

Boyce PJ, Disney MJ, Bleaken DG. 1999, *MNRAS* 302, 39

Boyle B. 1990, *MNRAS* 243, 231

Boyle BJ, Terlevich RJ. 1998, *MNRAS* 293, 49

Branch D. 1998, *Annu. Rev. Astron. Astrophys.* 36, 17

Bressan A, Chiosi C, Tantalo R. 1996, *Astron. Astrophys.* 311, 425

Brotherton MS, Van Breugel W, Smith RJ, Boyle BJ, Shanks T. 1998b, *Ap. J.* 505, 7

Brotherton MS, Wills BJ, Dey A, Van Breugal W, Antonucci R. 1998a, *Ap. J.* 501, 110

Brunner H, Mueller C, Friedrich P, Doerrer T, Staubert R, *et al.* 1997, *Astron. Astrophys.* 326, 885

Bruzual G, Barbuy B, Ortolani S, Bica E, Cuisinier F. 1997, *Astron. J.* 114, 1531

Bruzual G, Magris G. 1997, in the STScI Symp on the Hubble Deep Field, (astro-ph/9707154)

Burbidge G, Burbidge M. 1967, in Quasi-Stellar Objects, WH Freeman and Co.

Burles S, Tytler D. 1996, *Ap. J.* 460, 584

Carroll SM, Press WH. 1992, *Annu. Rev. Astron. Astrophys.* 30, 499

Carballo R, Sanchez SF, Gonzalas-Serrano JI, Benn CR, Vigotti M. 1998, *Astron. J.* 115, 1234

Castro S, Rich RM, McWilliam A, Ho LC, Spinrad H, *et al.* 1996, *Astron. J.* 111, 2439

Cavaliere A, Vittorini V. 1998, in The Young Universe, eds. S D'Odorico, A Fontana, E Giallongo, ASP Conf. Ser., 146, 28

Chatzichristou ET, Vanderriest C, Jaffe W. 1999, *Astron. Astrophys.* 343, 407

Cohen MH, Ogle PM, Tran HD, Vermeulen RC, Miller JS, *et al.* 1995, *Ap. J.* 448, L77

Collin S. 1998, preprint

Connolly AA, Szalay AS, Dickenson M, SubbaRao MU, Brunner RJ. 1997, *Ap. J.* 486, L11

Cozial R, Contini T, Davoust E, Considère S. 1997, *Ap. J.* 481, L67

Davidson K. 1977, *Ap. J.* 218, 20

Davidson K, Netzer H. 1979, Rev. Mod. Phys., 51, 715, (DN79).

de Freitas Pacheco JA. 1996, *MNRAS* 278, 841

Dey A, Spinrad H, Stern D, Graham JR, Chaffee FH. 1998, *Ap. J.* 498, L93

Djorgovski SG. 1998, in Fundamental Parameters of Cosmology, ed. Y Giroud-Hèraud, (Gif sur Yvette:Editions Frontières), in press

Edmunds MG. 1992, in Elements and the Cosmos, eds. MG Edmunds, R Terlevich, (Cambridge Univ. Press:New York), p.289

Ellis R, Smail I, Dressler A, Couch WJ, Oemler WJ, *et al.* 1997, *Ap. J.* 483, 582

Faber SM. 1973, *Ap. J.* 179, 423

Faber SM, Wegner G, Burstein D, Davies RL, Dressler A, *et al.* 1989, *Ap. J. Suppl.* 69, 763

Feltzing S, Gilmore G. 1998, in Galaxy Evolution: Connecting the Distant Universe with the Local Fossil Record, p. 71

Ferland GJ. 1999, in Quasars as Standard Candles for Cosmology, eds. J Baldwin, GJ Ferland, KT Korista, in press

Ferland GJ, Baldwin JA, Korista KT, Hamann F, Carswell RF, *et al.* 1996, *Ap. J.* 461, 683

Ferland GJ, Korista KT, Verner DA, Ferguson JW, Kingdon JB, *et al.* 1998, *PASP* 110,

761
Ferland GJ, Persson SE. 1989, *Ap. J.* 347, 656
Ferland GJ, Peterson BM, Horne K, Welsch WF, Nahar SN. 1992, *Ap. J.* 387, 95
Ferland GJ, Shields GA. 1985, in Astrophysics of Active Galaxies and Quasi-Stellar Objects, ed. JS Miller, Univ. Sci. Books, p. 157
Fisher D, Franx M, Illingworth G. 1995, *Ap. J.* 448, 119
Foltz CB, Chaffee F, Weymann RJ, Anderson SF. 1988, in QSO Absorption Lines: Probing the Universe, eds. JC Blades, DA Turnshek, CA Norman (Cambridge: Cambridge Univ Press), p. 53
Foltz CB, Weymann RJ, Peterson BM, Sun L, Malkan MA, *et al.* 1986, *Ap. J.* 307, 504
Franceschini A, Gratton R. 1997, *MNRAS* 286, 235
Francis PJ, Koratkar A. 1995, *MNRAS* 274, 504
Franx M, Illingworth GD. 1990, *Ap. J.* 359, L41
Franx M, Illingworth GD, Kelson DD, Van Dokkum PG, Tran K. 1997, *Ap. J.* 486, 75
Friaca ACS, Terlevich RJ. 1998, *MNRAS* 298, 399
Friaca ACS, Terlevich RJ. 1999, *MNRAS* in press
Frisch H. 1984, in Methods in Radiative Transfer, ed. W Kalkofen (Cambridge:Cambridge Univ. Press), 65
Gallagher SC, Brandt WN, Sambruna RM, Mathur S, Yamasaki N. 1999, *Ap. J.* in press
Ganguly R, Eracleous M, Charlton JC, Churchill CW. 1999, *Astron. J.* in press
Garnett DR. 1990, *Ap. J.* 363, 142
Gaskell CM, Shields GA, and Wampler EJ. 1981, *Ap. J.* 249, 443
Geisler D, Friel DE. 1992, *Astron. J.* 104, 128
Giavalisco M, Steidel CC, Macchetto FD. 1996, *Ap. J.* 470, 189
Gnedin NY, Ostriker JP. 1997, *Ap. J.* 486, 581
Goodrich RW, Miller JS. 1995, *Ap. J.* 448, L73
Gorgas J, Efstathiou G, Aragón Salamanca AA. 1990, *MNRAS* 245, 217
Grandi SA. 1981, *Ap. J.* 251, 451
Gratton RG. 1991, in Evolution of Stars: The Photospheric Abundance Connection, eds. G. Michaud, AV Tutukov, IAU Symp. 145, (Montreal:Univ. Montreal), 27
Green PJ, Aldcroft TL, Mathur S, Shartel N. 1997, *Ap. J.* 484, 135
Green PJ, Mathur S. 1996, *Ap. J.* 462, 637
Greggio L, and Renzini A. 1983 *Astron. Astrophys.* 118, 217
Grevesse N, Anders E. 1989, in Cosmic Abundances of Matter, AIP Conf. Proc. 183, ed. CI Waddington (New York:AIP), 1
Grillmair CJ, Turnshek DA. 1987, in QSO Absorption Lines: Probing the Universe, Poster Papers, eds. JC Blades, C Norman, DA Turnshek, p. 1
Guilloteau S, Omont A, McMahon RG, Cox P, Petitjean P. 1997, *Astron. Astrophys.* 328, L1
Haas M, Chini R, Maisenheimer K, Stickel M, Lemke D, *et al.* 1998, *Ap. J.* 503, L109
Haehnelt MG, Natarajan P, Rees MJ. 1998, *MNRAS* 300, 817
Haehnelt MG, Rees MJ. 1993, *MNRAS* 263, 168
Haiman Z, Loeb A. 1998, *Ap. J.* 503, 505
Hamann F. 1997, *Ap. J. Suppl.* 109, 279 (H97)
Hamann F. 1998, *Ap. J.* 500, 798

Hamann F, Barlow TA, Beaver EA, Burbidge EM, Cohen RD, *et al.* 1995, *Ap. J.* 443, 606

Hamann F, Barlow TA, Junkkarinen V. 1997c, *Ap. J.* 478, 87

Hamann F, Barlow TA, Cohen RD, Junkkarinen V, Burbidge EM. 1997b, *Ap. J.* 478, 80 (H97b)

Hamann F, Barlow TA, Cohen RD, Junkkarinen V, Burbidge EM. 1997e, in Mass Ejection From AGN, eds. R Weymann, I Shlosman, N Arav, ASP Conf. Series, 128, 187

Hamann F, Beaver EA, Cohen RD, Junkkarinen V, Lyons RW, *et al.* . 1997d, *Ap. J.* 488, 155

Hamann F, Chaffee R, Weymann RJ, Barlow TA, Junkkarinen VT. 1999b, in prep.

Hamann F, Cohen RD, Shields JC, Burbidge EM, Junkkarinen VT, *et al.* 1998, ApJ, 496, 761

Hamann F, Ferland GJ. 1992, ApJL, 391, L53

Hamann F, Ferland GJ. 1993a, Rev. Mex. Astr. Astrof., 26, 53

Hamann F, Ferland GJ. 1993b, *Ap. J.* 418, 11, (HF93b)

Hamann F, Korista KT. 1996, *Ap. J.* 464, 158

Hamann F, Korista KT, Ferland GJ. 1999a, in prep.

Hamann F, Korista KT, Morris SL. 1993, *Ap. J.* 415, 541

Hamann F, Shields JC, Cohen RD, Junkkarinen VT, Burbidge EM. 1997a, in Emission Lines From Active Galaxies: New Methods and Techniques, IAU Col. 159, eds. BM Peterson, F-Z Cheng, AS Wilson, ASP Conf. Ser., 113, 96

Hartquist TW, Snijders MAJ. 1982, Nature, 299, 783

Heap SR, Brown TM, Hubeny I, Landsman W, Yi S, *et al.* 1998, *Ap. J.* 492, L131

Hines DC, Low FJ, Thompson RI, Weymann RJ, Storrie-Lombardi LJ. 1999, *Ap. J.* 512, 140

Hines DC, Wills BJ. 1995, *Ap. J.* 448, L69

Hu EM, Cowie LL, McMahon RG. 1998, *Ap. J.* 502, L99

Idiart TP, De Freitas Pacheco JA, Costa RDD. 1996, *Astron. J.* 112, 2541

Isaac KG, McMahon RG, Hills RE, Withington S. 1994, *MNRAS* 269, 28

Isotov YI, Thuan TX. 1999, *Ap. J.* in press

Israelian G, López RJG, Rebolo R. 1998, *Ap. J.* 507, 805

Ivison RJ, Dunlop JS, Hughes DH, Archibald EN, Stevens JA, *et al.* 1998, *Ap. J.* 494, 211

Jablonka P, Alloin D, Bica E. 1992, *Astron. Astrophys.* 260, 97

Jablonka P, Martin P, Arimoto N. 1996, *Astron. J.* 112, 1415

Johansson S, Jordan C. 1984, *MNRAS* 210, 239

Jenkins EB. 1996, *Ap. J.* 471, 292

Jin L, Arnett WD, Chakrabarti SK. 1989, *Ap. J.* 336, 572

Junkkarinen VT. 1980, Ph.D. Dissertation, University of California – San Diego

Junkkarinen VT. 1998, private comm.

Junkkarinen VT, Beaver EA, Burbidge EM, Cohen RC, Hamann F, *et al.* 1997, in Mass Ejection From AGN, eds. R Weymann, I Shlosman, N Arav, ASP Conf. Series, 128, 220

Junkkarinen VT, Burbidge EM, Smith HE. 1983, *Ap. J.* 265, 51

Junkkarinen VT, Burbidge EM, Smith HE. 1987, *Ap. J.* 317, 460

Katz N, Quinn T, Bertschinger E, Gelb JM. 1994, *MNRAS* 270, L71

Kauffmann G. 1996, *MNRAS* 281, 487

King JR. 1993, *Astron. J.* 106, 1206

Kinney AL, Rivolo AR, Koratkar AR. 1990, *Ap. J.* 357, 338

Kirkman D, Tytler D. 1997, *Ap. J.* 489, L123

Kobulnicky HA, Skillman ED. 1998, *Ap. J.* 497, 601

Kodama T, Arimoto N. 1997, *Astron. Astrophys.* 320, 41

Köppen J, Arimoto N. 1990, *Astron. Astrophys.* 240, 22

Korista KT, Alloin D, Barr P, Clavel J, Cohen RD, *et al.* 1995, *Ap. J. Suppl.* 97, 285

Korista KT, Baldwin JA, Ferland GJ. 1998, *Ap. J.* 507, 24

Korista KT, Baldwin JA, Ferland GJ, Verner D. 1997b, *Ap. J. Suppl.* 108, 401

Korista KT, Ferland GJ, Baldwin BA. 1997a, *Ap. J.* 487, 555

Korista KT, Hamann F, Ferguson J, Ferland GJ. 1996, *Ap. J.* 461, 641

Korista KT, Voit GM, Morris SL, Weymann RJ. 1993, *Ap. J. Suppl.* 88, 357

Korista KT, Weymann RJ, Morris SL, Kopko M, Turnshek DA, *et al.* 1992, *Ap. J.* 401, 529

Kormendy J, Bender R, Evans AS, Richstone D. 1998, *Astron. J.* 115, 1823

Krolik J, Voit GM. 1998, *Ap. J.* 497, L5

Kundt W. 1996, *Astrophys. Sp. Sci.* 235, 319

Kundtschner H, Davies RL. 1997, *MNRAS* 295, L29

Kwan J. 1990, *Ap. J.* 353, 123

Kwan J, Krolik J. 1981, *Ap. J.* 250, 478, (KK81)

Laor A. 1998, in Quasars as Standard Candles for Cosmology, eds. J Baldwin, GJ Ferland, KT Korista, in press

Laor A, Bahcall JN, Jannuzi BT, Schneider DP, Green RF. 1995, *Ap. J. Suppl.* 99, 1

Laor A, Jannuzi BT, Green RF, Boroson TA. 1997, *Ap. J.* 489, 656

Larson RJ. 1974, *MNRAS* 169, 229

Loeb A. 1993, *Ap. J.* 404, L37

Loeb A, Rasio FA. 1994, *Ap. J.* 432, 52

Lowenthal JD, Koo DC, Guzman R, Gallego J, Phillips AC. 1997, *Ap. J.* 481, 673

Lu L, Sargent WLW, Barlow TA. 1998, *Astron. J.* 115, 55

Lu L, Sargent WLW, Barlow TA, Churchhill CW, Vogt SS. 1996, *Ap. J. Suppl.* 107, 475

Lu L, Savage BD. 1993, *Ap. J.* 403, 127

Madau P, Ferguson HC, Dickenson ME, Giavalisco M, Steidel CC, *et al.* 1996, *MNRAS* 283, 1388

Magain P. 1989, *Astron. Astrophys.* 209, 211

Magorrian J, Tremaine S, Richstone D, Bender R, Bower G, *et al.* 1998, *Astron. J.* 115, 2285

Mathews WG, Capriotti ER. 1985, in Astrophysics of Active Galaxies and Quasi-Stellar Objects, ed. JS Miller, Univ. Sci. Books, p. 183

Matteucci F. 1994, *Astron. Astrophys.* 288, 57

Matteucci F, Brocato E. 1990, *Ap. J.* 365, 539

Matteucci F, Francois P. 1989, *MNRAS* 239, 885

Matteucci F, Greggio L. 1986, *Astron. Astrophys.* 154, 279

Matteucci F, Tornambè A. 1987. *Astron. Astrophys.* 185, 51

McCarthy PJ. 1993, *Annu. Rev. Astron. Astrophys.* 31, 639

McLeod KK, Rieke GH 1995, *Ap. J.* 454, L77

McLeod KK, Rieke GH, Storrie-Lombardi LJ. 1999, *Ap. J.* 511, L67

McLure RJ, Dunlop JS, Kukula MJ, Baum SA, O'Dea CP, *et al.* 1998, preprint (astro-ph/9809030)

McWilliam A, Rich RM. 1994, *Ap. J. Suppl.* 91, 749

Mihalas D. 1978, Stellar Atmospheres, WH Freeman & Co., (San Francisco:Univ. Chicago Press)

Miller J, Tran H, Sheinis A. 1996, BAAS, 28, 1031

Minniti D, Olszewski EW, Liebert J, White SD, Hill JM, *et al.* 1995, *MNRAS* 277, 1293

Miralda-Escudé J, Rees MJ. 1997, *Ap. J.* 478, L57

Möller P, Jakobsen P, Perryman MAC. 1994, *Astron. Astrophys.* 287, 719

Morris SL, Weymann RJ, Foltz CB, Turnshek DA, Shectman S, *et al.* 1986, *Ap. J.* 310, 40

Murray N, Chiang J, Grossman SA, Voit GM. 1995, *Ap. J.* 451, 498

Mushotzky RF, Loewenstein M. 1997, *Ap. J.* 481, L63

Netzer H. 1990, in Active Galactic Nuclei, eds. RD Blandford, H Netzer, L Woltjer, (Berlin:Springer), 57

Netzer H, Brotherton MS, Wills BJ, Han M, Baldwin JA, *et al.* 1995, 448, 27

Netzer H, Wills BJ. 1983, *Ap. J.* 275, 445

Nissen PE, Gustafsson B, Edvardsson B, Gilmore G. 1994, *Astron. Astrophys.* 285, 440

Omont A, Petitjean P, Guilloteau S, McMahon RG, Solomon PM. 1996, Nature, 382, 428

Ortolani S, Renzini A, Gilmozzi R, Marconi G, Barbuy B, *et al.* 1996, in Formation of the Galactic Halo...Inside and Out, Eds. H Morrison, A Sarajedini, ASP Conf. Ser., 92, 96

Osmer PS. 1980, *Ap. J.* 237, 666

Osmer PS. 1998, in The Young Universe, eds. S D'Odorico, A Fontana, E Giallongo, ASP Conf. Ser., 146, 1

Osmer PS, Porter AC, Green RF. 1994, *Ap. J.* 436, 678

Osmer PS, Shields, JC. 1999, in Quasars as Standard Candles for Cosmology, eds. J Baldwin, GJ Ferland, KT Korista, in press

Osmer PS, Smith MG. 1976, *Ap. J.* 210, 276

Osmer PS, Smith MG. 1977, *Ap. J.* 213, 607

Osterbrock DE. 1977, *Ap. J.* 215, 733

Osterbrock DE. 1989, Astrophysics of Gaseous Nebulae and Active Galactic Nuclei, University Science Press

Peimbert M. 1967, *Ap. J.* 150, 825

Penston M. 1987, *MNRAS* 229, 1P

Peterson BM. 1993, *PASP* 105, 1084

Petitjean P, Rauch M, Carswell RF. 1994, *Astron. Astrophys.* 291, 29

Petitjean P, Srianand R. 1999, *Astron. Astrophys.* in press

Pettini M, King DL, Smith LJ, Hunstead RW. 1997, *Ap. J.* 486, 665

Phillips MM. 1977, *Ap. J.* 215, 746

Phillips MM. 1978, *Ap. J.* 226, 736

Prochaska JX, Wolfe AM. 1998, *Ap. J.* 507, 113

Prochaska JX, Wolfe AM. 1999, *Ap. J.* in press

Rauch M. 1998, *Annu. Rev. Astron. Astrophys.* 36, 267

Rauch M, Haehnelt MG, Steinmetz M. 1997, *Ap. J.* 481, 601

Renzini A. 1997, *Ap. J.* 488, 35

Renzini A. 1998, in The Young Universe, eds. S D'Odorico, A Fontana, E Giallongo, ASP Conf. Ser., 146, 298

Rich RM. 1988, *Astron. J.* 95, 828

Rich RM. 1990, *Ap. J.* 362, 604

Richards GT, York DG, Yanny B, Kollgaard RI, Laurent-Muehleisen SA, *et al.* 1999, *Ap. J.* in press

Saikia D, Kulkarni AR. 1998, *MNRAS* 298, L45

Sansom AE, Proctor RN. 1998, *MNRAS* 297, 953

Savage BD, Sembach KR. 1991, *Ap. J.* 379, 245

Savage BD, Tripp TM, Lu L. 1998, *Astron. J.* 115, 436

Savaglio S, Cristiani S, D'Odorico S, Fontana A, Giallong E, *et al.* 1997, *Astron. Astrophys.* 318, 347

Savaglio S, D'Odorico S, Mö ller P. 1994, *Astron. Astrophys.* 281, 331

Scalo JM. 1990, in Windows on Galaxies, eds. G Fabbiano, JS Gallagher, A Renzini, (Dordrecht:Kluwer Academic Publishers) p. 125

Schmidt GD, Hines DC. 1999, *Ap. J.* in press

Schneider DP. 1998, in Science with NGST, eds. EP Smith, A Koratkar, ASP Conf. Ser., 133, 106

Schneider DP, Schmidt M, and Gunn JE. 1991, *Astron. J.* 102, 837

Searle L, Zinn R. 1978, *Ap. J.* 225, 357

Shaver PA, Hook IM, Jackson CA, Wall JV, Kellerman KI. 1998, in Highly redshifted Radio Lines, eds. C Carilli, S Radford, K Menton, G. Langston, (PASP:San Francisco), in press

Shields GA. 1976, *Ap. J.* 204, 330

Shields GA. 1996, *Ap. J.* 461, L9

Shields JC, Ferland GJ, Peterson, BM. 1995, *Ap. J.* 441, 507

Shields JC, Hamann F, Foltz CB, Chaffee FH. 1997, in Emission Lines in Active Galaxies, eds. BM Peterson, F-Z Cheng, ASP Conf. Ser., 113, 118

Shklovskii IS. 1965, Sov. Astr., 8, 635

Sigut TAA, Pradhan AK. 1998, *Ap. J.* 499, L139

Sil'chenko OK, Burenkov AN, Vlasyuk VV. 1998, *Astron. Astrophys.* 337, 349

Silk J, Rees MJ. 1998, *Astron. Astrophys.* 331, L1

Songalia A, Cowie LL. 1996, *Astron. J.* 112, 335

Spaans M, Corollo CM. 1997, *Ap. J.* 482, L93

Spinrad H, Dey A, Stern D, Dunlop J, Peacock J, *et al.* 1997, *Ap. J.* 484, 581

Srianand R, Shankaranarayanan S. 1999, *Ap. J.* in press

Stanford SA, Eisenhardt PR, Dickenson M. 1998, *Ap. J.* 492, 461

Steidel CC, Adelberger KL, Dickenson M, Giavalisco M, Pettini M, *et al.* 1998, *Ap. J.* 492, 428

Steidel CC, Adelberger KL, Giavalisco M, Dickenson M, Pettini M. 1999, *Ap. J.* in press

Taniguchi Y, Arimoto N, Murayama T, Evans AS, Sanders DB, *et al.* 1997, in Quasar Hosts, eds. DL Clements, I Perez-Fouron, ESO-IAC Conf. Pro., p. 127

Taniguchi Y, Ikeuchi S, Shioya Y. 1999, *Ap. J.* 514, L12

Tantalo R, Chiosi C, Bressan A. 1998, *Astron. Astrophys.* 333, 419

Telfer RC, Kriss GA, Zheng W, Davidsen AF, Green RF. 1999, *Ap. J.* in press

Terndrup DM, Sadler EM, Rich RR. 1995, *Astron. J.* 110, 1774

Terlevich RJ, Boyle BJ. 1993, *MNRAS* 262, 491

Thomas D, Greggio L, & Bender R. 1998, *MNRAS* in press

Thompson KL, Hill GJ, Elston R. 1999, *Ap. J.* in press

Thuan TX, Izotov YI, Lipovetsky VA. 1995, *Ap. J.* 445, 108

Thurston TR, Edmunds MG, Henry RB. 1996, *MNRAS* 283, 990

Tiede GP, Frogel JA, Terndrup DM. 1995, *Astron. J.* 110, 2788

Tinsley B. 1979, *Ap. J.* 229, 1046

Tinsley B. 1980, Fund. of Cosmic Phys., 5, 287

Trager SC, Faber SM, Dressler A, Oemler A. 1997, *Ap. J.* 485, 92

Tripp TM, Lu L, Savage BD. 1996, *Ap. J. Suppl.* 102, 239

Tripp TM, Lu L, Savage BD. 1997, *Ap. J. Suppl.* 112, 1

Türler M, Courvoisier TJ-L. 1997, *Astron. Astrophys.* 329, 863

Turner EL. 1991, *Astron. J.* 101, 5

Turnshek DA. 1981, Ph.D. Dissertation, University of Arizona

Turnshek DA. 1984, 280, 51

Turnshek DA. 1986, in Quasars, eds. G. Swarup, VK Kapahi, IAU Symp. No. 119, (Dordrecht: Reidel), p. 317

Turnshek DA, Briggs FH, Foltz CB, Grillmair CJ, Weymann RJ. 1987, in QSO Absorption Lines: Probing the Universe, Poster Papers, eds. JC Blades, C Norman, DA Turnshek, p. 1

Turnshek DA. 1988, in QSO Absorption Lines: Probing the Universe, eds. JC Blades, C Norman, DA Turnshek, (Cambridge: Cambridge Univ Press), p. 17

Turnshek DA. 1994, in QSO Asborption Lines, ed. G Meylan, (Springer-Verlag), p. 223

Turnshek DA. 1997, in Mass Ejection From AGN, eds. R Weymann, I Shlosman, N Arav, ASP Conf. Series, 128, 193

Turnshek DA, Kopko M, Monier E, Noll D, Espey B, *et al.* 1996, *Ap. J.* 463, 110

Turnshek DA, Monier EM, Christopher JS, Espey BR. 1997, *Ap. J.* 476, 40

Tytler D, Fan XM, Burles S, Cottrell L, Davis C, *et al.* 1995, in QSO Absorption Lines, ed. G Meylan, (Garching:ESO), 289

Uomoto A. 1984, ApJ 284, 497

Van Dokkum PG, Franx M, Kelson DD, Illingworth GD. 1998, *Ap. J.* 504, L17

Van Zee L, Skillman ED, Salzer JJ. 1998, *Ap. J.* 497, L1

Vazdekis A, Peletier RF, Beckman JE, Casuso E. 1997, *Ap. J. Suppl.* 111, 203

Verner EM, Verner DA, Korista KT, Ferguson JW, Hamann F, *et al.* 1999, *Ap. J.* in press

Vila-Costas MB, Edmunds MG. 1993, *MNRAS* 265, 199

Voit GM, 1997, in Mass Ejection From AGN, eds. R Weymann, I Shlosman, N Arav, ASP Conf. Series, 128, 200

Voit GM, Weymann RJ, Korista KT. 1993, ApJ 413, 95

Wampler EJ, Bergeron J, Petitjean P. 1993, *Astron. Astrophys.* 273, 15

Wampler EJ, Chugai NN, Petitjean P. 1995, *Ap. J.* 443, 586

Warren SJ, Hewett PC, Osmer PS. 1994, *Ap. J.* 421, 412

Weymann RJ. 1994, in QSO Asborption Lines, ed. G Meylan, (Springer-Verlag), p. 213

Weymann RJ. 1997, in Mass Ejection From AGN, eds. R Weymann, I Shlosman, N Arav, ASP Conf. Series, 128, 3

Weymann RJ, Foltz C. 1983, in Quasars and Gravitational Lenses, 24th Liege Int. Astrophy. Coll., (Univ. de Liege:Belgium), p. 538

Weymann RJ, Turnshek DA, Christiansen WA. 1985, in Astrophysics of Active Galaxies and Quasi-Stellar Objects, ed. J Miller, (Mill Valley, CA: University Science Books), 185

Weymann RJ, Morris SL, Foltz CB, Hewett PC. 1991, *Ap. J.* 373, 23

Weymann RJ, Carswell RF, Smith MGA. 1981, *Annu. Rev. Astron. Astrophys.* 19, 41

Weymann RJ, Stern D, Bunker A, Spinrad H, Chaffee FH, *et al.* 1998, *Ap. J.* 505, L95

Weymann RJ, Williams RE, Peterson BM, Turnshek DA. 1979, *Ap. J.* 218, 6 19

Wheeler JC, Sneden C, Truran JW. 1989, *Annu. Rev. Astron. Astrophys.* 27, 279

Williams RE. 1971, *Ap. J.* 167, L27

Williams RE, Strittmatter PA, Carswell RF, Craine ER. 1975, *Ap. J.* 202, 296

Williams RE, Weymann RJ. 1976, *Ap. J.* 207, L143

Will BJ, Netzer H. 1983, *Ap. J.* 275, 445

Wills BJ, Netzer H, and Wills D. 1985, *Ap. J.* 288, 94

Wills BJ, Thompson KL, Han M, Netzer H, Wills D, *et al.* 1995, *Ap. J.* 447, 139

Worthey G, Faber SM, Gonzalez J. 1992, *Ap. J.* 398, 69

Yoshii Y, Tsujimoto T, Kawara K. 1998, *Ap. J.* 507, L113

Yoshii Y, Tsujimoto T, Nomoto K. 1996, *Ap. J.* 462, 266

Young P, Sargent WLW, and Boksenberg A. 1982, *Ap. J. Suppl.* 48, 455

Zaritsky D, Kennicutt RC, Huchra JP. 1994, *Ap. J.* 420, 87

Zheng W, Kriss GA, Davidsen AF. 1995, *Ap. J.* 440, 606

Zheng W, Kriss GA, Telfer RC, Grimes JP, Davidsen AF. 1997, *Ap. J.* 475, 469

Ziegler BL, Bender R. 1997, *MNRAS* 291, 527

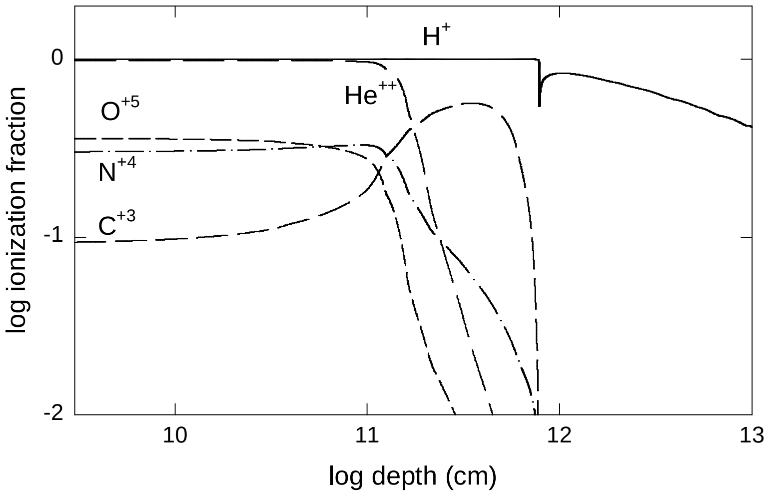
H^{+}
He^{++}
O^{+5}
N^{+4}
C^{+3}
0
-1
-2
log ionization fraction
10
11
12
13
log depth (cm)

Fig 3

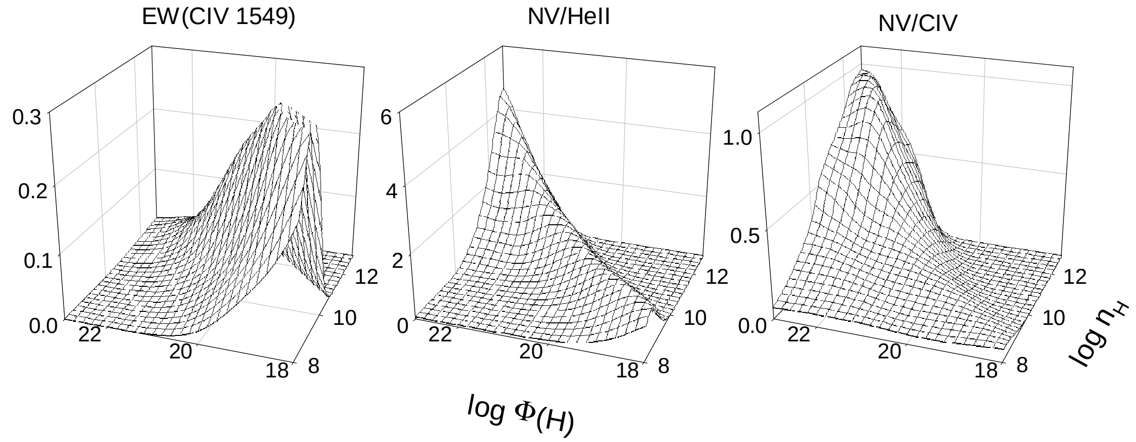
EW(CIV 1549)
NV/HeII
NV/CIV
0.3
0.2
0.1
0.0
6
4
2
0
1.0
0.5
0.0
22
20
18
8
10
12
log Φ(H)
log n$_H$

Fig 4

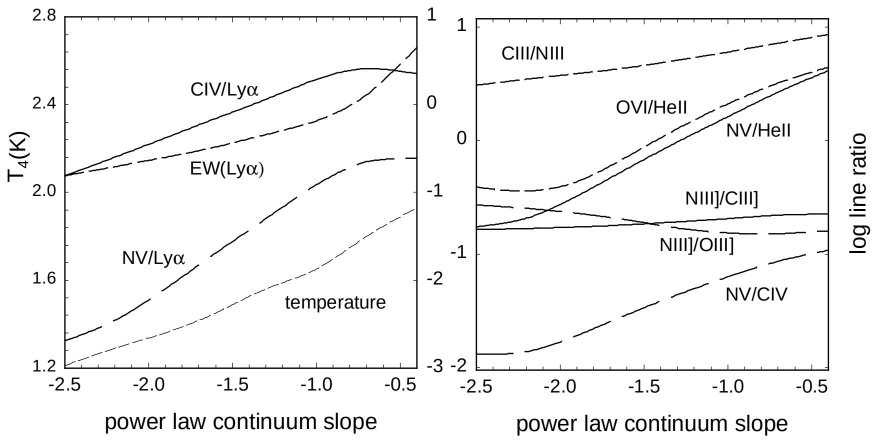
2.8
2.4
2.0
1.6
1.2
T_4(K)
1
0
-1
-2
-3
CIV/Lyα
EW(Lyα)
NV/Lyα
temperature
-2.5
-2.0
-1.5
-1.0
-0.5
power law continuum slope
1
0
-1
-2
CIII/NIII
OVI/HeII
NV/HeII
NIII]/CIII]
NIII]/OIII]
NV/CIV
-2.5
-2.0
-1.5
-1.0
-0.5
power law continuum slope
log line ratio

Fig 5

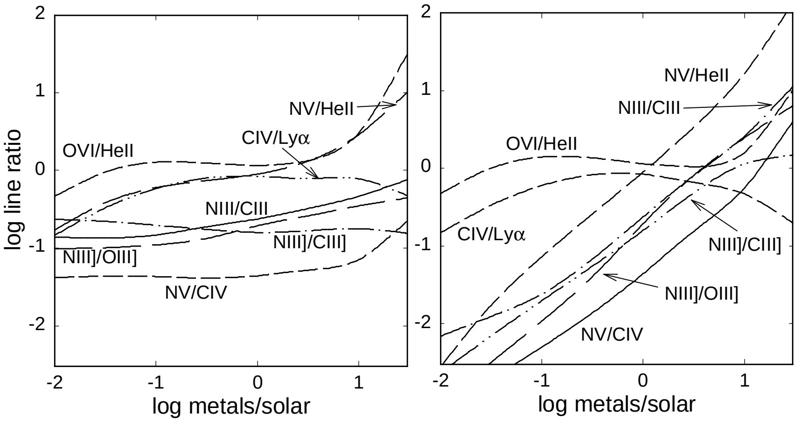
2
1
0
-1
-2
log line ratio
NV/HeII
CIV/Lyα
OVI/HeII
NIII/CIII
NIII]/OIII]
NIII]/CIII]
NV/CIV
-2
-1
0
1
log metals/solar
2
1
0
-1
-2
NV/HeII
NIII/CIII
OVI/HeII
CIV/Lyα
NIII]/CIII]
NIII]/OIII]
NV/CIV
-2
-1
0
1
log metals/solar

Fig 6

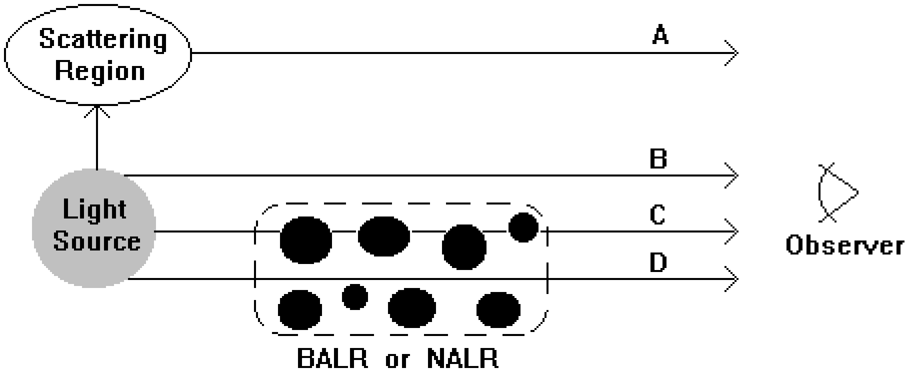
Scattering Region
A
B
Light Source
C
D
Observer
BALR or NALR